Cross section measurement of $e^+e^- \to \eta\psi(2S)$ and search for $e^+e^- \to \eta\tilde{X}(3872)$

M. Ablikim *et al.*[*]
(BESIII Collaboration)

(Received 26 March 2024; accepted 26 April 2024; published 5 June 2024)

The energy-dependent cross section for $e^+e^- \to \eta\psi(2S)$ is measured at 18 center of mass energies from 4.288 to 4.951 GeV using the BESIII detector. Using the same data samples, we also perform the first search for the reaction $e^+e^- \to \eta\tilde{X}(3872)$, but no evidence is found for the $\tilde{X}(3872)$ in the $\pi^+\pi^- J/\psi$ mass distribution. At each of the 18 center of mass energies, upper limits at the 90% confidence level on the cross section for $e^+e^- \to \eta\psi(2S)$ and on the product of the $e^+e^- \to \eta\tilde{X}(3872)$ cross section with the branching fraction of $\tilde{X}(3872) \to \pi^+\pi^- J/\psi$ are reported.

DOI: 10.1103/PhysRevD.109.112004

I. INTRODUCTION

Since the $X(3872)$ state was first observed by the Belle experiment in 2003 [1], abundant unexpected charmoniumlike states, such as the $Y(4260)$, $Z_c(3900)$, and $Z_{cs}(3985)$ states, have been discovered by the Belle, *BABAR*, BESIII, and CLEO experiments [2,3]. Their properties differ from conventional charmonia and do not match predictions based on potential model calculations for the charmonium spectrum [4]. Therefore, these states are collectively known as the "XYZ" particles and regarded as exotic states. They are still not well understood and have many theoretical interpretations, including compact tetraquarks, molecules, hybrids, and hadrocharmonia [2,5–10], among others.

Extensive experimental measurements of the production and decays of such states are essential for the understanding of their internal structures and for deepening our understanding of the low-energy properties of the strong interaction. Over the past two decades, several vector charmoniumlike states, including the $Y(4260)$ [11–15], $Y(4360)$ [16–18], and $Y(4660)$ [17,18], have been observed in the processes $e^+e^- \to \pi^+\pi^- J/\psi$ and $\pi^+\pi^-\psi(2S)$. In addition to these two processes through $\pi\pi$ hadronic transitions, other hadronic transitions of these Y states to lower mass charmonia [$J/\psi, \psi(2S)$, $\chi_{cJ}(J = 0, 1, 2)$, h_c, etc.] provide further insight into their internal structures.

Besides the decays to the above mentioned hidden-charm final states, Y states have also been discovered in the processes of e^+e^- annihilating to open-charm final states, such as $e^+e^- \to Y(4230) \to D^0D^{*-}\pi^+ + \text{c.c.}$ [19], $e^+e^- \to Y(4360) \to D^+D^-\pi^+\pi^-$ [20], and $e^+e^- \to Y(4660) \to D_s^+D_{s1}(2536)^-$ [21]. Very recently, the $Y(4230)$, $Y(4500)$, and $Y(4660)$ states have been observed in the process $e^+e^- \to D^{*0}D^{*-}\pi^+$ for the first time by BESIII [22], where the $Y(4500)$ is compatible with the state observed in $e^+e^- \to K^+K^- J/\psi$ [23].

Since the BESIII experiment observed the $Y(4230)$ in the $e^+e^- \to \eta J/\psi$ and $\eta' J/\psi$ processes, it follows that the process $e^+e^- \to \eta\psi(2S)$ can be an important way to search for Y states. The CLEO-c experiment searched for this process using data at a single center of mass (c.m.) energy $\sqrt{s} = 4.260$ GeV, but it did not observe a signal. Using a total of 5.25 fb^{-1} of e^+e^- collision data with c.m. energies from 4.236 to 4.600 GeV, BESIII reported the first observation of the process $e^+e^- \to \eta\psi(2S)$ with a statistical significance of 4.9 standard deviations [24]. In the past two years, BESIII has collected more data at c.m. energies above 4.600 GeV. In this work, we update the measurement for the cross sections of $e^+e^- \to \eta\psi(2S)$ with the new data samples.

In addition, we search for the $\tilde{X}(3872)$ state reported by the COMPASS experiment [25]. This state has quantum numbers $J^{PC} = 1^{+-}$ and a mass of 3860 MeV/c^2, therefore, it is regarded as the partner state of the $X(3872)$, since their masses and widths are close to each other but with different C parities. Inspired by Ref. [25], we search for the $\tilde{X}(3872)$ in the process $e^+e^- \to \eta\tilde{X}(3872)$, with $\tilde{X}(3872) \to \pi^+\pi^- J/\psi$. The similar process $e^+e^- \to \eta X(3872)$ is forbidden because the quantum numbers of $X(3872)$ are 1^{++}.

In this article, we analyze the data collected with the BESIII detector [26] at c.m. energies from 4.288 to 4.951 GeV; the corresponding c.m. energies and luminosities are listed in tables for the results of measured cross

[*]Full author list given at the end of the article.

sections described below. The energies were measured using $e^+e^- \to \mu^+\mu^-$ events with an uncertainty of 0.8 MeV [27], while the integrated luminosities were measured using Bhabha scattering events with an uncertainty of 1.0% [28,29]. We reconstruct the $e^+e^- \to \eta\psi(2S)/\tilde{X}(3872)$ signal process using the decays $\psi(2S)/\tilde{X}(3872) \to \pi^+\pi^- J/\psi$, $J/\psi \to \ell^+\ell^-$ ($\ell = e$ or μ), and $\eta \to \gamma\gamma$.

II. BESIII DETECTOR AND MONTE CARLO SIMULATION

The BESIII detector records symmetric e^+e^- collisions provided by the BEPCII storage ring [30] in the c.m. energy range from 2.00 to 4.95 GeV, with a peak luminosity of 1×10^{33} cm^{-2} s^{-1} achieved at $\sqrt{s} = 3.77$ GeV. BESIII has collected large data samples in this energy region [31–33]. The cylindrical core of the BESIII detector consists of a helium-based multilayer drift chamber, a plastic scintillator time-of-flight system (TOF), and a CsI(Tl) electromagnetic calorimeter (EMC), which are all enclosed in a superconducting solenoidal magnet providing a 1.0 T magnetic field. The solenoid is supported by an octagonal flux-return yoke with resistive plate chamber muon identifier modules interleaved with steel. The acceptance of charged particles and photons is 93% over 4π solid angle. The charged-particle momentum resolution at 1 GeV/c is 0.5%, and the dE/dx resolution is 6% for the electrons from Bhabha scattering events. The EMC measures photon energies with a resolution of 2.5% (5%) at 1 GeV in the barrel (end cap) region. The time resolution of the TOF barrel part is 68 ps. The end cap TOF system was upgraded in 2015 with multigap resistive plate chamber technology, used for the data taking of this analysis, providing a time resolution of 60 ps [34–36].

Simulated data samples produced with a Geant4-based [37] Monte Carlo (MC) package, which includes the geometric description of the BESIII detector and the detector response, are used to determine detection efficiencies and to estimate background contributions. The beam energy spread, the initial state radiation (ISR), and the vacuum polarization in the e^+e^- annihilations are simulated by using the generator KKMC [38,39].

Signal MC samples for the processes $e^+e^- \to \eta\psi(2S)$ and $\eta\tilde{X}(3872)$ are generated using helicity-amplitude [40,41] and phase-space [40,41] models, respectively, with 200,000 events at each c.m. energy. The mass of $\tilde{X}(3872)$ is 3860.0 ± 10.4 MeV/c^2 and the upper limit of $\tilde{X}(3872)$ width at 90% confidence level (CL) is 51 MeV [25], measured from the COMPASS measurement. We study two different scenarios for the $\tilde{X}(3872)$ width. In setting I, the mass and width of $\tilde{X}(3872)$ are set to 3860.0 MeV/c^2 and 51 MeV based on the COMPASS result [25], respectively; in setting II, the width is set to 1.19 MeV based on the $X(3872)$ width quoted from the Particle Data Group (PDG) [42], and the mass is scanned with a step of 1.5 MeV/c^2 in the mass interval from 3849.5 to 3870.5 MeV/c^2. Under these two different assumptions, the $e^+e^- \to \eta\tilde{X}(3872)$ cross sections are measured with the same methods. The results from the COMPASS $\tilde{X}(3872)$ mass 3860.0 MeV/c^2 are presented in the text as examples.

An inclusive MC sample at $\sqrt{s} = 4.682$ GeV is used to estimate possible background contributions. It is 40 times the size of the data sample and includes the production of open-charm processes, the ISR production of vector charmonium(like) states, and the continuum processes incorporated in KKMC. The known decay modes are modeled with EvtGen [40,41] using branching fractions taken from the PDG [42], and the remaining unknown charmonium decays are modeled with Lundcharm [43,44]. Final-state radiation from charged final-state particles is incorporated using PHOTOS [45]. Exclusive MC samples for some background processes are also generated at each c.m. energy to study their line shapes.

III. ANALYSIS OF $e^+e^- \to \eta\psi(2S)$

A. Event selection

The criteria applied in this analysis to select charged tracks and photons are described in Ref. [24]. Candidate events are required to have four charged tracks with zero net charge and at least two photon candidates. The pions and leptons have distinct momentum distributions for the signal process, thus the charged particles with momenta less than 0.8 GeV/c in the laboratory frame are assigned to be $\pi^\pm$, whereas the ones with momenta greater than 1.0 GeV/c are assumed to be $\ell^\pm$. The EMC energy deposits of electron and muon candidates are required to be greater than 1.0 GeV and less than 0.4 GeV, respectively. Photon candidates are reconstructed from showers in the EMC crystals. The reconstructed energies for the clusters in the barrel ($|\cos\theta| < 0.80$) and the end caps ($0.86 < |\cos\theta| < 0.92$) of the EMC are required to be higher than 25 and 50 MeV, respectively. To eliminate showers associated with charged particles, the angle between the photon and any charged track is required to be greater than 10°. To suppress the electronic noise and energy deposits unrelated to the event, the time of the EMC shower is required to be $0 \le t \le 700$ ns with respect to the event start time.

To improve the mass resolution and suppress the background, charged tracks are required to originate from a common vertex, and a four-constraint (4C) kinematic fit imposing energy-momentum conservation under the hypothesis of $e^+e^- \to \gamma\gamma\pi^+\pi^-\ell^+\ell^-$ is performed. If there are more than two photons in an event, the combination of $\gamma\gamma\pi^+\pi^-\ell^+\ell^-$ with the smallest chi-square $\chi^2_{\rm 4C}$ is retained for further study. The $\chi^2_{\rm 4C}$ of surviving events is required to be less than 40.

To identify signal candidates that involve the J/ψ resonance, the $\ell^+\ell^-$ invariant mass is required to satisfy $3064.6 < M(\ell^+\ell^-) < 3140.8$ MeV/c^2, which is about 3

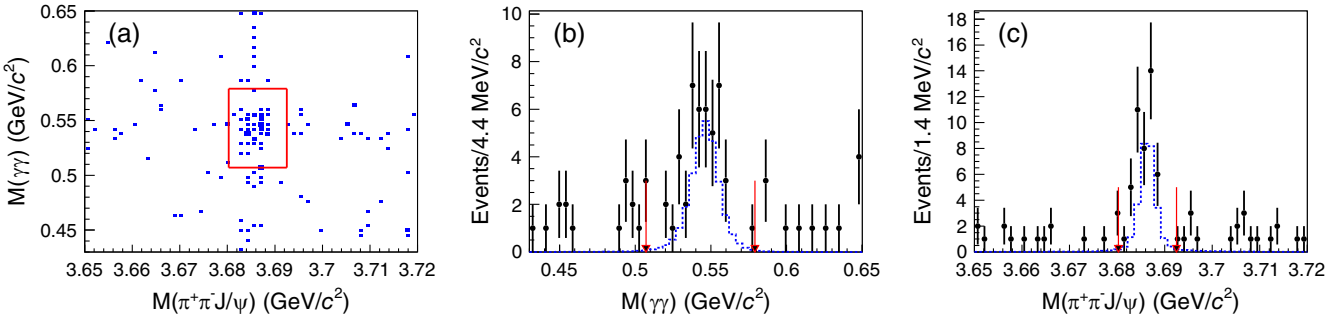

FIG. 1. (a) Distribution of $M(\gamma\gamma)$ versus $M(\pi^+\pi^- J/\psi)$, (b) the projection along $M(\gamma\gamma)$ in the $\psi(2S)$ mass window, and (c) the projection along $M(\pi^+\pi^- J/\psi)$ in the η mass window for the full dataset. The red rectangle and arrows represent the mass windows of η and $\psi(2S)$ selections, and the blue dashed histograms in (b) and (c) represent the $e^+e^- \to \eta\psi(2S)$ signal MC simulated shapes of $M(\gamma\gamma)$ and $M(\pi^+\pi^- J/\psi)$ distributions, respectively.

times the resolution of the J/ψ nominal mass. To remove the background events $e^+e^- \to \eta' J/\psi$ with $\eta' \to \pi^+\pi^-\eta$, the invariant mass of $\pi^+\pi^-\gamma\gamma$, $M(\pi^+\pi^-\gamma\gamma)$, is required to be greater than 1 GeV/c^2. At the energy points above 4.600 GeV, the invariant mass of $\gamma\gamma J/\psi$ is required to be greater than 3.74 GeV/c^2 to remove the backgrounds from the $e^+e^- \to \pi^+\pi^-\psi(2S)$ process.

After applying the aforementioned selection criteria, the invariant mass distributions of $M(\gamma\gamma)$ versus $M(\pi^+\pi^- J/\psi)$ for the full dataset, for $e^+e^- \to \eta\psi(2S)$ signal MC samples, and the corresponding projection plots are shown in Fig. 1. Here $M(\pi^+\pi^- J/\psi) = M(\pi^+\pi^-\ell^+\ell^-) - M(\ell^+\ell^-) + M(J/\psi)_{\rm PDG}$ is used to eliminate the detection resolution from $M(\ell^+\ell^-)$, and $M(\pi^+\pi^-\ell^+\ell^-)$ and $M(J/\psi)_{\rm PDG}$ are the invariant mass of $\pi^+\pi^-\ell^+\ell^-$ and the nominal mass of the J/ψ, respectively. The signal regions for the η and $\psi(2S)$ states are set to be $507.1 < M(\gamma\gamma) < 579.1$ and $3680.3 < M(\pi^+\pi^- J/\psi) < 3692.5$ MeV/c^2, respectively, quoted from Ref. [24] and within 3 times the detector deviations to the nominal masses of η and $\psi(2S)$ states [42]. Significant clusters from $e^+e^- \to \eta\psi(2S)$ signals can be seen in Fig. 1.

B. Background analysis

The same selection criteria are applied to the inclusive MC sample generated at $\sqrt{s} = 4.682$ GeV to investigate possible background contributions. The corresponding processes are listed in Table I. These backgrounds are divided into three categories: non-$\psi(2S)$ events (type I), non-η events (type II), and both non-η and non-$\psi(2S)$ events (type III). Figure 2 shows the $M(\gamma\gamma)$ versus $M(\pi^+\pi^- J/\psi)$ distributions for the three different background categories.

The dominant background contribution comes from the process $e^+e^- \to \gamma\gamma\psi(2S)$ with $\psi(2S) \to \pi^+\pi^- J/\psi$ and $J/\psi \to \ell^+\ell^-$, and its yield is measured directly in this analysis. After applying all the above selection criteria except from the η mass window, the $M(\gamma\gamma)$ distribution in the process $e^+e^- \to \gamma\gamma\psi(2S)$ is shown in Fig. 2(b) as an example. We can measure its yield by requiring that the mass of $\gamma\gamma$ is greater than 300 MeV/c^2 and not within $[507.1, 579.1]$ MeV/c^2. Here, these mass range requirements are applied to remove the contributions from the $e^+e^- \to \pi^0\psi(2S)$, $e^+e^- \to \gamma_{\rm ISR}\psi(2S)$, and $e^+e^- \to \eta\psi(2S)$ processes. The contribution from $e^+e^- \to \pi^0\pi^0\psi(2S)$ is negligible compared to $e^+e^- \to \gamma\gamma\psi(2S)$.

The number of $\gamma\gamma\psi(2S)$ events in the $\psi(2S)$ signal region but not in the η or π^0 signal region $[N^0_{\gamma\gamma\psi(2S)}]$ is obtained by subtracting the number of observed events in the $\psi(2S)$ sideband regions $[N^{\rm o}_{\rm side}]$ from the number of observed events in $\psi(2S)$ signal region $[N^{\rm o}_{\rm sig}]$, i.e., $N^0_{\gamma\gamma\psi(2S)} = N^{\rm o}_{\rm sig} - N^{\rm o}_{\rm side}$. The number of $e^+e^- \to \gamma\gamma\psi(2S)$

TABLE I. List of the possible background processes in the $e^+e^- \to \eta\psi(2S)$ signal region (where $J/\psi \to \ell^+\ell^-$).

Type	Decay mode (branching fraction)		
I	$e^+e^- \to \pi^+\pi^-\psi(2S)$,	$\psi(2S) \to J/\psi\eta$ (3.37%),	$\eta \to \gamma\gamma$ (39.41%)
II	$e^+e^- \to \pi^0\pi^0\psi(2S)$,	$\psi(2S) \to \pi^+\pi^- J/\psi$ (34.68%),	
	$e^+e^- \to \gamma\gamma\psi(2S)$,	$\psi(2S) \to \pi^+\pi^- J/\psi$ (34.68%),	
III	$e^+e^- \to \pi^+\pi^-\psi(2S)$,	$\psi(2S) \to \gamma\chi_{cJ}(J = 0, 1, 2)$ (9.79%, 9.75%, 9.52%),	$\chi_{cJ} \to \gamma J/\psi$ (1.4%, 34.3%, 19.0%)
	$e^+e^- \to \omega\chi_{cJ}(J = 0, 1, 2)$,	$\omega \to \pi^+\pi^-\pi^0$ (89.3%),	$\chi_{cJ} \to \gamma J/\psi$ (1.4%, 34.3%, 19.0%)
	$e^+e^- \to \phi\chi_{cJ}(J = 0, 1, 2)$,	$\phi \to \pi^+\pi^-\pi^0$ (15.24%),	$\chi_{cJ} \to \gamma J/\psi$ (1.4%, 34.3%, 19.0%)
	$e^+e^- \to \gamma X(3872)$,	$X(3872) \to \omega J/\psi$ (2.3%),	$\omega \to \pi^+\pi^-\pi^0$ (89.3%)

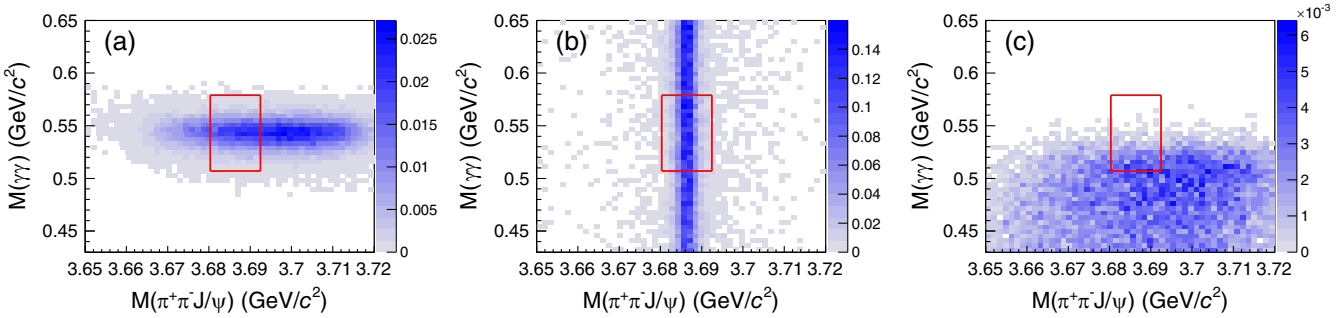

FIG. 2. Distributions of $M(\gamma\gamma)$ versus $M(\pi^+\pi^- J/\psi)$ for the exclusive background MC samples of (a) type I, $e^+e^- \to \pi^+\pi^-\psi(2S)$, $\psi(2S) \to J/\psi\eta$ at $\sqrt{s} = 4.288$ GeV; (b) type II, $e^+e^- \to \gamma\gamma\psi(2S)$ at $\sqrt{s} = 4.682$ GeV; and (c) type III, $e^+e^- \to \pi^+\pi^-\psi(2S), \psi(2S) \to \gamma\chi_{c1}$ at $\sqrt{s} = 4.288$ GeV. The MC samples are normalized to the numbers of the observed events in data at the corresponding energy points. The red rectangles represent the mass windows of η and $\psi(2S)$ selections.

events in the η and $\psi(2S)$ signal regions $[N^1_{\gamma\gamma\psi(2S)}]$ is obtained from the $N^0_{\gamma\gamma\psi(2S)}$ as follows:

$$N^1_{\gamma\gamma\psi(2S)} = F \cdot N^0_{\gamma\gamma\psi(2S)}. \quad (1)$$

We define a factor F from branching fractions and selection efficiencies as

$$F = \frac{\epsilon^1_e \mathcal{B}_e + \epsilon^1_\mu \mathcal{B}_\mu}{\epsilon^0_e \mathcal{B}_e + \epsilon^0_\mu \mathcal{B}_\mu}, \quad (2)$$

where ϵ^1_e and ϵ^1_μ are the detection efficiencies of $e^+e^- \to \gamma\gamma\psi(2S)$ background events for the $J/\psi \to e^+e^-$ and $J/\psi \to \mu^+\mu^-$ decay channels in the η and $\psi(2S)$ signal regions, respectively; ϵ^0_e and ϵ^0_μ are the detection efficiencies of $e^+e^- \to \gamma\gamma\psi(2S)$ background events for the $J/\psi \to e^+e^-$ and $J/\psi \to \mu^+\mu^-$ decay channels in the $\psi(2S)$ signal region but outside the η and π^0 signal regions, respectively; $\mathcal{B}_e$ and $\mathcal{B}_\mu$ are the branching fractions of decays $J/\psi \to e^+e^-$ and $J/\psi \to \mu^+\mu^-$, respectively [42]. The values related to the $e^+e^- \to \gamma\gamma\psi(2S)$ backgrounds are listed in Table II. The uncertainty on F is neglected since it is very small.

The yields for each of the other background processes in the signal region $(N_{\mathrm{bkg},i})$ are calculated using

$$N_{\mathrm{bkg},i} = \mathcal{L}_{\mathrm{int}}(1+\delta)_i |1-\Pi|^{-2} \epsilon_i \mathcal{B}_i \sigma^{\mathrm{B}}_{\mathrm{bkg},i}, \quad (3)$$

where i represents each background channel; $\mathcal{L}_{\mathrm{int}}$ is the integrated luminosity; $|1-\Pi|^{-2}$ is the vacuum polarization factor [46]; ϵ_i and $\mathcal{B}_i$ are the selection efficiency and the product branching fraction of the intermediate states taken from the PDG [42] for the ith background mode, respectively; and $\sigma^{\mathrm{B}}_{\mathrm{bkg},i}$ is the measured Born cross section of the ith background mode. The production cross sections for these background processes are taken from Refs. [47–55]. Assuming an input line shape from Refs. [47–55], the ISR correction factor $(1+\delta)_i$ is obtained from a quantum electrodynamics calculation [56] using the KKMC generator [38,39].

The total number of background events (n^{b}) in the signal region of $e^+e^- \to \eta\psi(2S)$ is obtained by

$$n^{\mathrm{b}} = \sum_i N_{\mathrm{bkg},i} + N^1_{\gamma\gamma\psi(2S)}. \quad (4)$$

TABLE II. The numbers of $e^+e^- \to \gamma\gamma\psi(2S)$ events outside $[N^0_{\gamma\gamma\psi(2S)}]$ and inside $[N^1_{\gamma\gamma\psi(2S)}]$ the η signal region, the F factor, and the numbers of observed events in the signal $[N^{\mathrm{o}}_{\mathrm{sig}}]$ and sideband $[N^{\mathrm{o}}_{\mathrm{side}}]$ regions of the $\psi(2S)$ mass window at each c.m. energy. The statistical uncertainty of $N^0_{\gamma\gamma\psi(2S)}$ is calculated by the Feldman-cousins method [57].

$\sqrt{s}$ (GeV)	F	$N^{\mathrm{o}}_{\mathrm{sig}}$	$N^{\mathrm{o}}_{\mathrm{side}}$	$N^0_{\gamma\gamma\psi(2S)}$	$N^1_{\gamma\gamma\psi(2S)}$
4.288	0.246	6	6	$0.00^{+3.28}_{-0.00}$	$0.00^{+0.81}_{-0.00}$
4.312	0.265	4	0	$4.00^{+2.78}_{-1.66}$	$1.06^{+0.74}_{-0.44}$
4.337	0.265	7	0	$7.00^{+3.31}_{-2.74}$	$1.86^{+0.88}_{-0.73}$
4.377	0.243	2	1	$1.00^{+2.26}_{-0.86}$	$0.24^{+0.55}_{-0.21}$
4.396	0.237	10	0	$10.00^{+3.81}_{-3.22}$	$2.37^{+0.90}_{-0.76}$
4.436	0.209	8	0	$8.00^{+3.32}_{-2.70}$	$1.67^{+0.69}_{-0.56}$
4.612	0.141	1	0	$1.00^{+1.76}_{-0.63}$	$0.14^{+0.25}_{-0.09}$
4.628	0.134	4	1	$3.00^{+2.78}_{-1.66}$	$0.40^{+0.37}_{-0.22}$
4.641	0.136	2	0	$2.00^{+2.26}_{-1.26}$	$0.27^{+0.31}_{-0.17}$
4.661	0.125	4	0	$4.00^{+2.78}_{-1.66}$	$0.50^{+0.35}_{-0.21}$
4.682	0.126	19	0	$19.00^{+4.83}_{-4.18}$	$2.39^{+0.61}_{-0.53}$
4.699	0.120	2	0	$2.00^{+2.26}_{-1.26}$	$0.24^{+0.27}_{-0.15}$
4.740	0.110	0	0	$0.00^{+1.29}_{-0.00}$	$0.00^{+0.14}_{-0.00}$
4.750	0.106	5	0	$5.00^{+2.81}_{-2.24}$	$0.53^{+0.30}_{-0.24}$
4.781	0.100	7	0	$7.00^{+3.31}_{-2.74}$	$0.70^{+0.33}_{-0.27}$
4.843	0.087	5	1	$4.00^{+2.81}_{-2.24}$	$0.35^{+0.25}_{-0.20}$
4.918	0.077	4	0	$4.00^{+2.78}_{-1.66}$	$0.31^{+0.21}_{-0.13}$
4.951	0.075	0	0	$0.00^{+1.29}_{-0.00}$	$0.00^{+0.10}_{-0.00}$

TABLE III. The total numbers of background events in the signal region ($n^{\rm b}$) at different energy points for $e^+e^- \to \eta\psi(2S)$ signal process, together with the expected numbers of background events from different processes. Ellipses mean that the results are 0 or close to 0. Here the $e^+e^- \to \gamma\gamma\psi(2S)$ uncertainties are statistical only, while the uncertainties of the other backgrounds are the sum of the statistical and the systematic uncertainties in quadrature.

$\sqrt{s}$ (GeV)	4.288	4.312	4.337	4.377	4.396	4.436
$\pi^+\pi^-\psi(2S),\psi(2S)\to J/\psi\eta$	1.07 ± 0.09	0.23 ± 0.01	0.02	⋯	⋯	⋯
$\pi^+\pi^-\psi(2S),\psi(2S)\to\gamma\chi_{c0}$	0.02	0.01	⋯	⋯	⋯	⋯
$\pi^+\pi^-\psi(2S),\psi(2S)\to\gamma\chi_{c1}$	0.15 ± 0.01	0.07	0.01	⋯	⋯	⋯
$\pi^+\pi^-\psi(2S),\psi(2S)\to\gamma\chi_{c2}$	⋯	⋯	⋯	⋯	⋯	⋯
$\pi^0\pi^0\psi(2S)$	0.05 ± 0.01	0.07 ± 0.01	0.11 ± 0.01	0.19 ± 0.02	0.22 ± 0.03	0.21 ± 0.03
$\omega\chi_{c0}$	⋯	⋯	⋯	⋯	⋯	⋯
$\omega\chi_{c1}$	⋯	0.01 ± 0.01	0.01 ± 0.01	0.01 ± 0.01	0.01	0.01 ± 0.01
$\omega\chi_{c2}$	⋯	⋯	⋯	0.05 ± 0.02	0.06 ± 0.01	0.06 ± 0.01
$\gamma X(3872)$	⋯	⋯	⋯	⋯	⋯	⋯
$\gamma\gamma\psi(2S)$	$0.00^{+0.81}_{-0.00}$	$1.06^{+0.74}_{-0.44}$	$1.86^{+0.88}_{-0.73}$	$0.24^{+0.55}_{-0.21}$	$2.37^{+0.90}_{-0.76}$	$1.67^{+0.69}_{-0.56}$
$n^{\rm b}$	1.29 ± 0.81	1.45 ± 0.74	2.00 ± 0.88	0.50 ± 0.55	2.65 ± 0.90	1.95 ± 0.69

$\sqrt{s}$ (GeV)	4.612	4.628	4.641	4.661	4.682	4.699
$\phi\chi_{cJ}$	⋯	⋯	⋯	⋯	⋯	⋯
$\pi^0\pi^0\psi(2S)$	0.01 ± 0.00	0.07 ± 0.01	0.08 ± 0.01	0.10 ± 0.02	0.31 ± 0.04	0.07 ± 0.01
$\omega\chi_{cJ}$	⋯	⋯	⋯	⋯	⋯	⋯
$\gamma X(3872)$	⋯	⋯	⋯	⋯	⋯	⋯
$\gamma\gamma\psi(2S)$	$0.14^{+0.25}_{-0.09}$	$0.40^{+0.37}_{-0.22}$	$0.27^{+0.31}_{-0.17}$	$0.50^{+0.35}_{-0.21}$	$2.39^{+0.61}_{-0.53}$	$0.24^{+0.27}_{-0.15}$
$n^{\rm b}$	0.15 ± 0.25	0.48 ± 0.37	0.36 ± 0.31	0.61 ± 0.35	2.70 ± 0.61	0.31 ± 0.27

$\sqrt{s}$ (GeV)	4.740	4.750	4.781	4.843	4.918	4.951
$\phi\chi_{cJ}$	⋯	⋯	⋯	⋯	⋯	⋯
$\pi^0\pi^0\psi(2S)$	0.02 ± 0.01	0.03 ± 0.03	0.04 ± 0.03	0.02 ± 0.03	0.01 ± 0.01	⋯
$\omega\chi_{cJ}$	⋯	⋯	⋯	⋯	⋯	⋯
$\gamma X(3872)$	⋯	⋯	⋯	⋯	⋯	⋯
$\gamma\gamma\psi(2S)$	$0.00^{+0.14}_{-0.00}$	$0.53^{+0.30}_{-0.24}$	$0.70^{+0.33}_{-0.27}$	$0.35^{+0.24}_{-0.20}$	$0.31^{+0.21}_{-0.13}$	$0.00^{+0.10}_{-0.00}$
$n^{\rm b}$	0.02 ± 0.14	0.56 ± 0.30	0.74 ± 0.33	0.37 ± 0.25	0.31 ± 0.21	0.00 ± 0.10

Finally, the total numbers of background events in the signal region at different energy points, together with the numbers of background events from different decay processes, are listed in Table III. The uncertainties for the numbers of the $e^+e^- \to \gamma\gamma\psi(2S)$ events are statistical only, while for the other backgrounds events, they are the statistical and systematic uncertainties added in quadrature.

C. Cross section measurement

Since there are only a few events in the signal region of $e^+e^- \to \eta\psi(2S)$, the number of observed events ($n^{\rm obs}$), which is the sum of the number of expected background ($n^{\rm b}$) and signal (x) events, follows a Poisson distribution,

$$P(n^{\rm obs};x,n^{\rm b}) = \frac{(x+n^{\rm b})^{n^{\rm obs}}}{n^{\rm obs}!}e^{-(x+n^{\rm b})}. \quad (5)$$

In this analysis, the number of signal events $e^+e^- \to \eta\psi(2S)$ is obtained using the likelihood ratio ordering (also known as the Feldman-Cousins, F-C) method [57], i.e., the value of x corresponding to the maximum $P(n^{\rm obs};x,n^{\rm b})$. Thus, $n^{\rm sig} = \max(0, n^{\rm obs} - n^{\rm b})$ is the best estimation of the number of signal events in the physically allowed region.

The statistical uncertainty of the number of signal events at a 68.27% CL is estimated with the F-C method [57]. Since no significant $\eta\psi(2S)$ signals are observed at some of the energy points, the confidence intervals for the number of signal events with the lower and upper limits at a 90% CL are obtained with a toolkit which supports the F-C method and takes into account the systematic uncertainty, the Poissonian limit estimator (POLE) program [58].

The Born cross section of $e^+e^- \to \eta\psi(2S)$ is calculated by

$$\sigma^{\rm B}[e^+e^- \to \eta\psi(2S)] = \frac{n^{\rm sig}}{\mathcal{L}_{\rm int}(1+\delta)|1-\Pi|^{-2}\mathcal{B}_1\mathcal{B}_2(\epsilon_e\mathcal{B}_e+\epsilon_\mu\mathcal{B}_\mu)}, \quad (6)$$

TABLE IV. The cross sections $\sigma^{\rm B}$ and the confidence intervals with the lower and upper limits on $\sigma^{\rm B}$ with the POLE method ($\sigma^{\rm B}_{\rm POLE}$) for $e^+e^- \to \eta\psi(2S)$ at different energy points, together with integrated luminosities $\mathcal{L}_{\rm int}$, the numbers of observed events $n^{\rm obs}$, the background events $n^{\rm b}$, the signal events $n^{\rm sig}$, the confidence intervals with the lower and upper limits for the numbers of signal events $n^{\rm sig}_{\rm POLE}$, the products of detection efficiencies and branching fractions $\Sigma = \mathcal{B}_1\mathcal{B}_2(\epsilon_e\mathcal{B}_e + \epsilon_\mu\mathcal{B}_\mu)$, and the products of ISR correction factor and vacuum polarization factor $(1+\delta)|1-\Pi|^{-2}$. The uncertainties of $n^{\rm sig}$ and $\sigma^{\rm B}$ are statistical only. The lower and upper limits are given at 90% CL including the systematic uncertainties.

$\sqrt{s}$ (GeV)	$\mathcal{L}_{\rm int}$ (pb^{-1})	$n^{\rm obs}$	$n^{\rm b}$	$n^{\rm sig}$	$n^{\rm sig}_{\rm POLE}$	$\Sigma(10^{-2})$	$(1+\delta)\lvert1-\Pi\rvert^{-2}$	σ^B (pb)	$\sigma^{\rm B}_{\rm POLE}$ (pb)
4.288	491.5	6	1.29	$4.7^{+3.3}_{-2.2}$	(1.4, 0.1)	0.363	0.90	$2.9^{+2.0}_{-1.3}$	(0.9, 6.3)
4.312	492.1	4	1.45	$2.5^{+2.8}_{-1.6}$	(0.4, 7.5)	0.333	1.01	$1.5^{+1.7}_{-1.0}$	(0.2, 4.5)
4.337	501.1	4	2.00	$2.0^{+2.8}_{-1.6}$	(0.0, 7.2)	0.301	1.13	$1.2^{+1.6}_{-0.9}$	(0.0, 4.2)
4.377	522.8	6	0.50	$5.5^{+3.3}_{-2.2}$	(1.8, 12.0)	0.255	1.34	$3.1^{+1.8}_{-1.2}$	(1.0, 6.8)
4.396	505.0	3	2.65	$0.3^{+2.3}_{-0.3}$	(0.0, 5.2)	0.236	1.44	$0.2^{+1.3}_{-0.2}$	(0.0, 3.1)
4.436	568.1	9	1.95	$7.1^{+3.8}_{-2.7}$	(2.5, 14.3)	0.207	1.65	$3.6^{+2.0}_{-1.4}$	(1.3, 7.4)
4.612	103.7	0	0.15	$0.0^{+1.1}_{-0.0}$	(0.0, 2.4)	0.296	0.97	$0.0^{+3.9}_{-0.0}$	(0.0, 8.2)
4.628	521.5	0	0.48	$0.0^{+0.8}_{-0.0}$	(0.0, 2.4)	0.293	0.97	$0.0^{+0.6}_{-0.0}$	(0.0, 1.6)
4.641	551.7	2	0.36	$1.6^{+2.3}_{-1.1}$	(0.1, 5.5)	0.294	0.98	$1.0^{+1.4}_{-0.7}$	(0.1, 3.4)
4.661	529.4	2	0.61	$1.4^{+2.3}_{-1.0}$	(0.0, 5.3)	0.289	0.98	$0.9^{+1.5}_{-0.7}$	(0.0, 3.6)
4.682	1667.4	3	2.70	$0.3^{+2.3}_{-0.3}$	(0.0, 4.9)	0.290	0.98	$0.1^{+0.5}_{-0.1}$	(0.0, 1.0)
4.699	535.5	1	0.31	$0.7^{+1.8}_{-0.6}$	(0.0, 4.0)	0.291	0.98	$0.5^{+1.1}_{-0.4}$	(0.0, 2.6)
4.740	163.9	0	0.02	$0.0^{+1.3}_{-0.0}$	(0.0, 2.5)	0.297	0.99	$0.0^{+2.7}_{-0.0}$	(0.0, 5.2)
4.750	366.5	3	0.56	$2.4^{+2.3}_{-1.7}$	(0.5, 6.8)	0.296	0.99	$2.3^{+2.1}_{-1.5}$	(0.5, 6.3)
4.781	511.5	1	0.74	$0.3^{+1.8}_{-0.3}$	(0.0, 3.8)	0.295	0.99	$0.2^{+1.2}_{-0.2}$	(0.0, 2.5)
4.843	525.2	1	0.37	$0.6^{+1.8}_{-0.6}$	(0.0, 4.0)	0.294	1.00	$0.4^{+1.1}_{-0.4}$	(0.0, 2.6)
4.918	207.8	0	0.31	$0.0^{+1.0}_{-0.0}$	(0.0, 2.4)	0.288	1.01	$0.0^{+1.6}_{-0.0}$	(0.0, 4.0)
4.951	159.3	0	0.00	$0.0^{+1.3}_{-0.0}$	(0.0, 2.4)	0.285	1.01	$0.0^{+2.8}_{-0.0}$	(0.0, 5.3)

where $\mathcal{B}_1$ and $\mathcal{B}_2$ are the branching fractions of $\psi(2S) \to \pi^+\pi^- J/\psi$ and $\eta \to \gamma\gamma$ [42], respectively; ϵ_e and ϵ_μ are the detection efficiencies for e^+e^- and $\mu^+\mu^-$ modes, respectively; $(1+\delta)$ is the radiative correction factor obtained from the quantum electrodynamics calculation [56] using the KKMC generator [38,39], assuming that the cross section follows an input line shape of the $Y(4260)$ [42] at the energy points below 4.600 GeV and an input line shape in the form of a power function $1/s$ at the energy points above 4.600 GeV. The Born cross sections, the corresponding confidence intervals with the lower and upper limits at 90% CL, and the numbers used in the calculation are listed in Table IV.

Figure 3 shows the measured Born cross sections for $e^+e^- \to \eta\psi(2S)$ as a function of the c.m. energy. Due to the limited statistics, it is difficult to draw a clear conclusion whether the vector charmoniumlike states exist in the cross section distribution or not.

IV. ANALYSIS OF $e^+e^- \to \eta\tilde{X}(3872)$

A. Event selection

Since we search for the $\tilde{X}(3872)$ signals in the $e^+e^- \to \eta\tilde{X}(3872) \to \eta\pi^+\pi^- J/\psi$ process, with $\eta \to \gamma\gamma$ and $J/\psi \to e^+e^-$ or $\mu^+\mu^-$, the applied selections are similar to the ones used for the $e^+e^- \to \eta\psi(2S)$ process, except for the signal and sideband regions of $\tilde{X}(3872)$ applied in the $M(\pi^+\pi^- J/\psi)$ distribution.

The $\tilde{X}(3872)$ signal region in the $M(\pi^+\pi^- J/\psi)$ distribution for the setting I (setting II) is required to be within 2

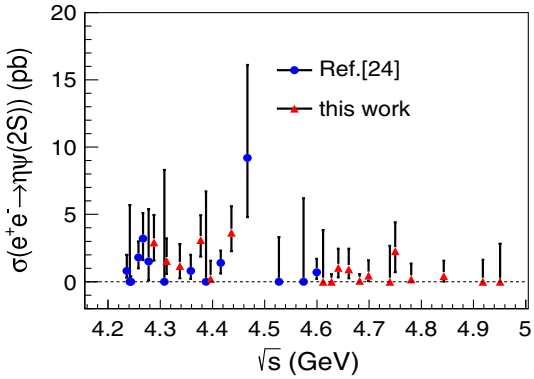

FIG. 3. The measured Born cross sections as a function of the c.m. energy. The blue dots and red triangles are from Ref. [24] and this measurement, respectively. The error bars represent the statistical errors only.

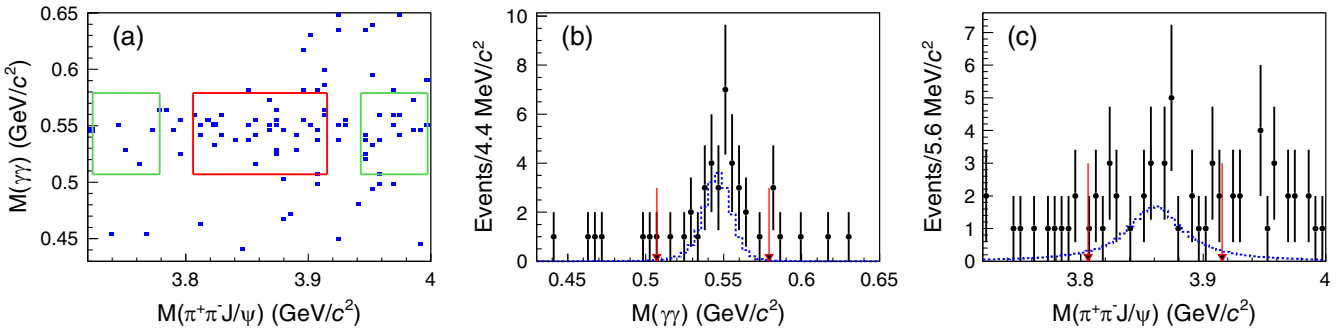

FIG. 4. (a) Distribution of $M(\gamma\gamma)$ versus $M(\pi^+\pi^- J/\psi)$, (b) the projection along $M(\gamma\gamma)$ in the $\tilde{X}(3872)$ mass window, and (c) the projection along $M(\pi^+\pi^- J/\psi)$ in the η mass window for the full data sample. The red rectangle and arrows represent the signal region, the green rectangles represent the sideband regions, and the blue dashed histograms in (b) and (c) represent the $e^+e^- \to \eta\tilde{X}(3872)$ signal MC simulated shapes of $M(\gamma\gamma)$ and $M(\pi^+\pi^- J/\psi)$ distributions for setting I, respectively.

(3) times the detector resolution from the COMPASS $\tilde{X}(3872)$ mass 3860.0 MeV/c^2, $3805.9 < M(\pi^+\pi^- J/\psi) < 3915.9\,\text{MeV}/c^2$ [$3849.5 < M(\pi^+\pi^- J/\psi) < 3871.3$ MeV/c^2]. The sideband regions are required to be within the range from 3 (4) to 5 (7) times the detector resolution around the known $\tilde{X}(3872)$ mass, $3723.5 < M(\pi^+\pi^- J/\psi) < 3778.4$ MeV/c^2 and $3943.4 < M(\pi^+\pi^- J/\psi) < 3998.4\,\text{MeV}/c^2$ [$3835.1 < M(\pi^+\pi^- J/\psi) < 3845.9\,\text{MeV}/c^2$ and $3874.9 < M(\pi^+\pi^- J/\psi) < 3885.7$ MeV/c^2]. Figure 4 shows the $M(\gamma\gamma)$ and $M(\pi^+\pi^- J/\psi)$ distributions for the full data sample, together with the corresponding projection plots. There is no evidence for $e^+e^- \to \eta\tilde{X}(3872)$ under either of the $\tilde{X}(3872)$ width assumptions.

B. Background analysis

The selection criteria are also applied to the inclusive MC sample at $\sqrt{s} = 4.682$ GeV to investigate possible background contributions, which are classified into peaking and nonpeaking background events. The sources of peaking background are listed in Table V, and Fig. 5 shows the $M(\gamma\gamma)$ versus $M(\pi^+\pi^- J/\psi)$ distributions for the $e^+e^- \to \pi^+\pi^-\psi(3823)$, $\psi(3823) \to \gamma\chi_{c1}$ background process [59] at $\sqrt{s} = 4.682$ GeV as an example. The expected numbers of the peaking background events in the signal ($n^{\rm b}_{\rm sig}$) and the sideband ($n^{\rm b}_{\rm side}$) regions of $\tilde{X}(3872)$ for settings I and II are calculated by Eq. (3) and listed in Tables VI and VII, respectively. The number of background events ($n^{\rm b}$) in the signal region is corrected by

TABLE V. List of the peaking background processes (where $J/\psi \to \ell^+\ell^-$).

Decay mode		
$e^+e^- \to \pi^+\pi^-\psi(3823)$,	$\psi(3823) \to \gamma\chi_{c1}$,	$\chi_{c1} \to \gamma J/\psi$
$e^+e^- \to \omega\chi_{cJ}(J = 0, 1, 2)$,	$\omega \to \pi^+\pi^-\pi^0$,	$\chi_{cJ} \to \gamma J/\psi$
$e^+e^- \to \phi\chi_{cJ}(J = 0, 1, 2)$,	$\phi \to \pi^+\pi^-\pi^0$,	$\chi_{cJ} \to \gamma J/\psi$

$$n^{\rm b} = n^{\rm b}_{\rm nonpeak} + n^{\rm b}_{\rm peak} = (n^{\rm obs}_{\rm side} - n^{\rm b}_{\rm side}) + n^{\rm b}_{\rm sig}, \quad (7)$$

where $n^{\rm obs}_{\rm side}$ is the number of observed events from the sideband regions of $e^+e^- \to \eta\tilde{X}(3872)$. The number of nonpeaking background events $n^{\rm b}_{\rm nonpeak}$ is represented by $n^{\rm obs}_{\rm side} - n^{\rm b}_{\rm side}$, and the number of peaking background events $n^{\rm b}_{\rm peak}$ is represented by $n^{\rm b}_{\rm sig}$.

The values of $n^{\rm b}_{\rm sig}$, $n^{\rm obs}_{\rm side}$, $n^{\rm b}_{\rm side}$, $n^{\rm b}$, and the number of observed events in the $\eta\tilde{X}(3872)$ signal region $n^{\rm obs}_{\rm sig}$ are listed in Table VIII for settings I and II.

C. Cross section measurement

The signal yield of $e^+e^- \to \eta\tilde{X}(3872)$, $n^{\rm sig}$, is obtained by $n^{\rm sig} = \max(0, n^{\rm obs}_{\rm sig} - n^{\rm b})$ according to the F-C method [57], and the upper limit is provided at 90% CL by the POLE method since no significant signal is observed. The statistical significance at each energy point is calculated using the P-value method and is summarized in Table VIII.

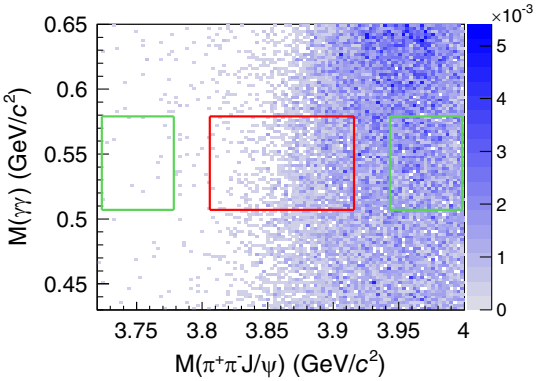

FIG. 5. Distribution of $M(\gamma\gamma)$ versus $M(\pi^+\pi^- J/\psi)$ from $e^+e^- \to \pi^+\pi^-\psi(3823)$, $\psi(3823) \to \gamma\chi_{c1}$ background MC sample at $\sqrt{s} = 4.682$ GeV, normalized to the number of the observed events of data. The red rectangle represents the signal region and the green rectangles represent the sideband regions.

TABLE VI. Expected numbers of different peaking background events in $e^+e^- \to \eta\tilde{X}(3872)$ signal and sideband regions at different energy points for setting I, where $n^{\rm b}_{\rm sig}$ and $n^{\rm b}_{\rm side}$ are the total sums for the signal and the sideband regions, respectively. Ellipses represent results close to 0 or 0.

	$\sqrt{s}$ (GeV)	$\phi\chi_{c1}$	$\phi\chi_{c2}$	$\omega\chi_{c1}$	$\omega\chi_{c2}$	$\pi^+\pi^-\psi(3823)$	$n^{\rm b}_{\rm sig}$
Signal region	4.612	⋯	⋯	0.02 ± 0.03	0.02	0.11 ± 0.14	0.15 ± 0.11
	4.628	0.01	0.01	0.08 ± 0.03	0.03	0.48 ± 0.26	0.61 ± 0.49
	4.641	0.01	0.01	0.10 ± 0.04	0.04	0.57 ± 0.22	0.73 ± 0.58
	4.661	⋯	0.01	0.07 ± 0.03	0.05 ± 0.03	0.54 ± 0.17	0.69 ± 0.55
	4.682	0.01	0.03 ± 0.01	0.05 ± 0.04	0.04 ± 0.05	0.64 ± 0.17	0.77 ± 0.64
	4.699	⋯	0.01	0.03 ± 0.01	0.02	0.07 ± 0.04	0.14 ± 0.08
	4.740	⋯	⋯	0.00 ± 0.01	0.01	0.01 ± 0.01	0.02 ± 0.01
	4.750	⋯	⋯	0.01	0.01	0.01 ± 0.01	0.04 ± 0.02
	4.780	⋯	⋯	0.00 ± 0.01	0.01 ± 0.01	0.01	0.02 ± 0.01
	4.843	⋯	⋯	⋯	0.00 ± 0.01	⋯	0.01 ± 0.01
	4.918	⋯	⋯	⋯	⋯	⋯	0.01
	$\sqrt{s}$ (GeV)	$\phi\chi_{c1}$	$\phi\chi_{c2}$	$\omega\chi_{c1}$	$\omega\chi_{c2}$	$\pi^+\pi^-\psi(3823)$	$n^{\rm b}_{\rm side}$
Sideband region	4.612	⋯	⋯	0.01 ± 0.02	0.01	0.01 ± 0.02	0.03 ± 0.02
	4.628	0.01	⋯	0.04 ± 0.02	0.02	0.14 ± 0.08	0.22 ± 0.15
	4.641	0.01	⋯	0.06 ± 0.02	0.02	0.28 ± 0.11	0.37 ± 0.29
	4.661	⋯	0.01	0.04 ± 0.02	0.03 ± 0.02	0.51 ± 0.16	0.60 ± 0.51
	4.682	0.01	0.03 ± 0.01	0.04 ± 0.03	0.03 ± 0.04	1.00 ± 0.27	1.12 ± 1.00
	4.699	⋯	0.02	0.03 ± 0.01	0.03	0.16 ± 0.09	0.24 ± 0.17
	4.740	⋯	⋯	0.01 ± 0.01	0.01	0.05 ± 0.07	0.07 ± 0.05
	4.750	⋯	⋯	0.01	0.01	0.16 ± 0.09	0.19 ± 0.16
	4.780	⋯	⋯	0.01 ± 0.01	0.01 ± 0.02	0.10 ± 0.06	0.12 ± 0.10
	4.843	⋯	⋯	⋯	0.00 ± 0.01	0.00 ± 0.01	0.01 ± 0.01
	4.918	⋯	⋯	⋯	⋯	⋯	0.01

TABLE VII. Expected numbers of different peaking background events in $e^+e^- \to \eta\tilde{X}(3872)$ signal and sideband regions at different energy points for setting II, where $n^{\rm b}_{\rm sig}$ and $n^{\rm b}_{\rm side}$ are the total sums for the signal and the sideband regions, respectively. Ellipses represent results close to 0 or 0.

	$\sqrt{s}$ (GeV)	$\phi\chi_{c2}$	$\omega\chi_{c1}$	$\omega\chi_{c2}$	$\pi^+\pi^-\psi(3823)$	$n^{\rm b}_{\rm sig}$
Signal region	4.612	⋯	0.00 ± 0.01	⋯	0.02 ± 0.03	0.03 ± 0.03
	4.628	⋯	0.02 ± 0.01	0.01	0.10 ± 0.06	0.13 ± 0.11
	4.641	⋯	0.02 ± 0.01	0.01	0.12 ± 0.05	0.16 ± 0.12
	4.661	⋯	0.02 ± 0.01	0.01 ± 0.01	0.10 ± 0.03	0.13 ± 0.10
	4.682	⋯	0.01 ± 0.01	0.01 ± 0.01	0.09 ± 0.02	0.12 ± 0.09
	4.699	⋯	0.01	⋯	0.01	0.02 ± 0.01
	4.740	⋯	⋯	⋯	⋯	⋯
	4.750	⋯	⋯	⋯	⋯	0.01
	$\sqrt{s}$ (GeV)	$\phi\chi_{c2}$	$\omega\chi_{c1}$	$\omega\chi_{c2}$	$\pi^+\pi^-\psi(3823)$	$n^{\rm b}_{\rm side}$
Sideband region	4.612	⋯	0.00 ± 0.01	⋯	0.02 ± 0.03	0.03 ± 0.02
	4.628	⋯	0.01 ± 0.01	0.01	0.10 ± 0.05	0.12 ± 0.10
	4.641	⋯	0.02 ± 0.01	0.01	0.11 ± 0.04	0.14 ± 0.11
	4.661	⋯	0.02 ± 0.01	0.01 ± 0.01	0.10 ± 0.03	0.13 ± 0.11
	4.682	0.01	⋯	0.01 ± 0.01	0.10 ± 0.03	0.13 ± 0.10
	4.699	⋯	0.01	⋯	0.01 ± 0.01	0.03 ± 0.01
	4.740	⋯	⋯	⋯	⋯	⋯
	4.750	⋯	⋯	⋯	⋯	0.01

TABLE VIII. The $\sigma^{\rm B}[e^+e^- \to \eta\tilde{X}(3872)]B[\tilde{X}(3872) \to \pi^+\pi^- J/\psi]$ (σB) values and the corresponding upper limits at 90% CL (UL) with the POLE method for settings I and II at different energy points, together with the integrated luminosity $\mathcal{L}_{\rm int}$, the numbers of observed events in signal $n^{\rm obs}_{\rm sig}$ and sideband $n^{\rm obs}_{\rm side}$ regions, the expected numbers of peaking background events in signal $n^{\rm b}_{\rm sig}$ and sideband $n^{\rm b}_{\rm side}$ regions, the total yield of background events in signal region $n^{\rm b} = n^{\rm obs}_{\rm side} + n^{\rm b}_{\rm sig} - n^{\rm b}_{\rm side}$, the numbers of signal events $n^{\rm sig}$, the upper limits at 90% CL of the number of signal events $n^{\rm sig}_{\rm POLE}$, the products of detection efficiencies and branching fractions $\Sigma = \mathcal{B}_2(\epsilon_e\mathcal{B}_e + \epsilon_\mu\mathcal{B}_\mu)$, the products of ISR correction factor and vacuum polarization factor $(1+\delta)|1-\Pi|^{-2}$, and the signal statistical significances. The uncertainties of $n^{\rm sig}$ and σB are statistical only. The significance is calculated using the P-value method.

	$\sqrt{s}$ (GeV)	$\mathcal{L}_{\rm int}$ (pb^{-1})	$n^{\rm obs}_{\rm sig}$	$n^{\rm obs}_{\rm side}$	$n^{\rm b}_{\rm sig}$	$n^{\rm b}_{\rm side}$	$n^{\rm b}$	$n^{\rm sig}$	$n^{\rm sig}_{\rm POLE}$	$\Sigma(10^{-2})$	$(1+\delta)\lvert1-\Pi\rvert^{-2}$	σB (pb)	UL (pb)	Significance
Setting I	4.612	103.7	1	0	0.13	0.03	0.11	$0.9^{+1.8}_{-0.6}$	(0.0, 4.2)	0.848	0.73	$1.4^{+2.7}_{-1.0}$	(0.0, 6.5)	1.2σ
	4.628	521.5	3	1	0.62	0.22	1.40	$1.6^{+2.3}_{-1.2}$	(0.0, 6.0)	0.835	0.79	$0.5^{+0.7}_{-0.4}$	(0.0, 1.8)	1.0σ
	4.641	551.7	5	0	0.72	0.37	0.35	$4.7^{+2.8}_{-2.2}$	(1.6, 9.6)	0.828	0.81	$1.3^{+0.8}_{-0.6}$	(0.4, 2.6)	4.0σ
	4.661	529.4	7	1	0.69	0.60	1.08	$5.9^{+3.3}_{-2.8}$	(2.4, 11.8)	0.788	0.84	$1.7^{+0.9}_{-0.8}$	(0.7, 3.4)	3.6σ
	4.682	1667.4	7	6	0.82	1.16	5.66	$1.3^{+3.3}_{-1.3}$	(0.0, 7.6)	0.765	0.86	$0.1^{+0.3}_{-0.1}$	(0.0, 0.7)	0.4σ
	4.699	535.5	2	3	0.12	0.21	2.91	$0.0^{+1.5}_{-0.0}$	(0.0, 3.7)	0.757	0.87	$0.0^{+0.4}_{-0.0}$	(0.0, 1.1)	⋯
	4.740	163.9	2	0	0.01	0.05	0.00	$2.0^{+2.3}_{-1.3}$	(0.5, 5.8)	0.750	0.89	$1.8^{+2.1}_{-1.2}$	(0.5, 5.3)	⋯
	4.750	366.5	4	2	0.02	0.17	1.85	$2.2^{+2.8}_{-1.6}$	(0.0, 7.1)	0.743	0.90	$0.9^{+1.1}_{-0.6}$	(0.0, 2.9)	1.2σ
	4.781	511.5	1	3	0.02	0.12	2.90	$0.0^{+0.5}_{-0.0}$	(0.0, 3.1)	0.738	0.91	$0.0^{+0.1}_{-0.0}$	(0.0, 0.9)	⋯
	4.843	525.2	0	3	0.00	0.01	2.99	$0.0^{+0.1}_{-0.0}$	(0.0, 2.4)	0.726	0.93	$0.0^{+0.0}_{-0.0}$	(0.0, 0.7)	⋯
	4.918	207.8	1	2	0.00	0.00	2.00	$0.0^{+1.0}_{-0.0}$	(0.0, 3.2)	0.714	0.95	$0.0^{+0.7}_{-0.0}$	(0.0, 2.2)	⋯
	4.951	159.3	0	0	0.00	0.00	0.00	$0.0^{+1.3}_{-0.0}$	(0.0, 2.4)	0.708	0.96	$0.0^{+1.2}_{-0.0}$	(0.0, 2.3)	⋯

	$\sqrt{s}$ (GeV)	$\mathcal{L}_{\rm int}$ (pb^{-1})	$n^{\rm obs}_{\rm sig}$	$n^{\rm obs}_{\rm side}$	$n^{\rm b}_{\rm sig}$	$n^{\rm b}_{\rm side}$	$n^{\rm b}$	$n^{\rm sig}$	$n^{\rm sig}_{\rm POLE}$	$\Sigma(10^{-2})$	$(1+\delta)\lvert1-\Pi\rvert^{-2}$	σB (pb)	UL (pb)	Significance
Setting II	4.612	103.7	0	0	0.03	0.03	0.00	$0.0^{+1.3}_{-0.0}$	(0.0, 2.4)	1.136	0.73	$0.0^{+1.5}_{-0.0}$	(0.0, 2.8)	⋯
	4.628	521.5	1	0	0.14	0.13	0.01	$1.0^{+1.8}_{-0.6}$	(0.0, 4.4)	1.119	0.79	$0.2^{+0.4}_{-0.1}$	(0.0, 1.0)	2.4σ
	4.641	551.7	0	1	0.15	0.14	1.02	$0.0^{+0.5}_{-0.0}$	(0.0, 2.4)	1.110	0.81	$0.0^{+0.1}_{-0.0}$	(0.0, 0.5)	⋯
	4.661	529.4	2	1	0.13	0.14	1.00	$1.0^{+2.3}_{-0.8}$	(0.0, 5.0)	1.083	0.84	$0.2^{+0.5}_{-0.2}$	(0.0, 1.0)	0.6σ
	4.682	1667.4	2	0	0.13	0.13	0.00	$2.0^{+2.3}_{-1.3}$	(0.5, 5.8)	1.063	0.86	$0.1^{+0.1}_{-0.1}$	(0.0, 0.4)	⋯
	4.699	535.5	1	0	0.02	0.02	0.00	$1.0^{+1.8}_{-0.6}$	(0.0, 4.3)	1.048	0.87	$0.2^{+0.4}_{-0.1}$	(0.0, 0.9)	⋯
	4.740	163.9	1	0	0.00	0.00	0.00	$1.0^{+1.8}_{-0.6}$	(0.0, 4.4)	1.044	0.89	$0.7^{+1.2}_{-0.4}$	(0.0, 2.9)	⋯
	4.750	366.5	0	1	0.00	0.00	1.00	$0.0^{+0.5}_{-0.0}$	(0.0, 2.4)	1.034	0.90	$0.0^{+0.2}_{-0.0}$	(0.0, 0.7)	⋯
	4.781	511.5	0	0	0.00	0.00	0.00	$0.0^{+1.3}_{-0.0}$	(0.0, 2.4)	1.032	0.91	$0.0^{+0.3}_{-0.0}$	(0.0, 0.5)	⋯
	4.843	525.2	0	0	0.00	0.00	0.00	$0.0^{+1.3}_{-0.0}$	(0.0, 2.4)	1.018	0.93	$0.0^{+0.3}_{-0.0}$	(0.0, 0.5)	⋯
	4.918	207.8	1	0	0.00	0.00	0.00	$1.0^{+1.8}_{-0.6}$	(0.0, 4.3)	0.999	0.95	$0.5^{+0.9}_{-0.3}$	(0.0, 2.2)	3.1σ
	4.951	159.3	0	0	0.00	0.00	0.00	$0.0^{+1.3}_{-0.0}$	(0.0, 2.4)	0.981	0.96	$0.0^{+0.9}_{-0.0}$	(0.0, 1.6)	⋯

The product of the $e^+e^- \to \eta\tilde{X}(3872)$ cross section and the $\tilde{X}(3872) \to \pi^+\pi^- J/\psi$ branching fraction, together with the upper limit at 90% CL, are calculated by

$$\sigma^{\rm B}[e^+e^- \to \eta\tilde{X}(3872)]B[\tilde{X}(3872) \to \pi^+\pi^- J/\psi] = \frac{n^{\rm sig}}{\mathcal{L}_{\rm int}(1+\delta)|1-\Pi|^{-2}\mathcal{B}_2(\epsilon_e\mathcal{B}_e + \epsilon_\mu\mathcal{B}_\mu)}, \quad (8)$$

where $(1+\delta)$ is the radiative correction factor obtained from the quantum electrodynamics calculation [56] using the KKMC generator [38,39], assuming that the c.m. energy dependence cross section follows the line shape of the power function $1/s$.

The $\sigma^{\rm B}[e^+e^- \to \eta\tilde{X}(3872)]B[\tilde{X}(3872) \to \pi^+\pi^- J/\psi]$ values, the corresponding upper limits at 90% CL, together with the other information used for the cross section calculation, are listed in Table VIII, separately for settings I and II. In setting II, the results from the mass set at other positions are measured with the same methods. Their statistical significances are less than 3σ. The $\sigma^{\rm B}[e^+e^- \to \eta\tilde{X}(3872)]B[\tilde{X}(3872) \to \pi^+\pi^- J/\psi]$ upper limits at 90% CL for the two settings are shown in Fig. 6.

V. SYSTEMATIC UNCERTAINTIES

The systematic uncertainties for the cross section measurements of the $e^+e^- \to \eta\psi(2S)$ and $e^+e^- \to \eta\tilde{X}(3872)$ $[\tilde{X}(3872) \to \pi^+\pi^- J/\psi]$ processes are mainly due to the integrated luminosity, the tracking and photon reconstruction, the branching fractions of intermediate particle decays, the ISR correction factor, the kinematic

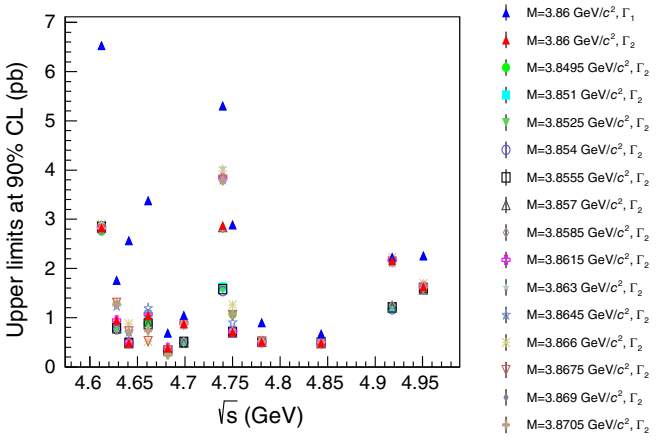

FIG. 6. Upper limits of $\sigma^{\mathrm{B}}[e^+e^- \to \eta\tilde{X}(3872)]B[\tilde{X}(3872) \to \pi^+\pi^- J/\psi]$ at 90% CL for different assumptions of the $\tilde{X}(3872)$ widths (Γ) and masses (M). The widths of 51 and 1.19 MeV are represented by Γ_1 and Γ_2, respectively. The blue and red triangles are the results from settings I and II with the COMPASS $\tilde{X}(3872)$ mass 3.86 GeV/c^2, respectively. Other markers represent the results from the assumptions of the $\tilde{X}(3872)$ width with 1.19 MeV and the masses scanned with a step of 1.5 MeV/c^2 in the mass interval from 3849.5 to 3870.5 MeV/c^2.

fit, the background estimation, and the mass windows. These systematic uncertainties are explained below and summarized in Tables IX and X. The total systematic uncertainty is obtained by summing the individual uncertainties in quadrature, assuming that all sources are independent.

(i) Luminosity. The uncertainty of integrated luminosity is 1.0%, measured using Bhabha scattering events [28,29].

(ii) Tracking efficiency. The uncertainty of the tracking efficiency is 1.0% per single track from Ref. [60]. Since there are four charged tracks in the $e^+e^- \to \eta\psi(2S)$ and $\eta\tilde{X}(3872)$ final states, the total uncertainty due to tracking efficiency is 4.0%.

(iii) Photon detection efficiency. The uncertainty from photon reconstruction is 1.0% per photon, from the study of the process $J/\psi \to \rho^0\pi^0, \rho^0 \to \pi^+\pi^-, \pi^0 \to \gamma\gamma$ [61]. Thus the total uncertainty due to photon reconstruction is 2.0%.

(iv) Branching fraction. The uncertainties on the branching fractions of the intermediate states from $e^+e^- \to \eta\psi(2S)$ and $e^+e^- \to \eta\tilde{X}(3872) \to \eta\pi^+\pi^- J/\psi$ are 1.2% and 0.8%, respectively, from the PDG values [42].

(v) ISR correction factor. The ISR factors are obtained from the input line shapes of the $Y(4260)$ state at the energy points below 4.600 GeV and the power function $1/s$ at the energy points above 4.600 GeV. To estimate the uncertainties, the input line shapes are replaced by the $\psi(4415)$ state at the energy points below 4.600 GeV and the $Y(4660)$ states at the energy points above 4.600 GeV; the $(1+\delta)\epsilon$ differences for the different assumptions are taken as the systematic uncertainties, and they range from 0.2% to 18.3%.

(vi) Kinematic fit. The systematic uncertainty from the kinematic fit is estimated by correcting the helix

TABLE IX. The systematic uncertainties of $e^+e^- \to \eta\psi(2S)$ cross section measurement for luminosity (Lum), tracking efficiency, photon reconstruction efficiency, branching fraction (BR), ISR correction factor, kinematic fit (KMFIT), background estimation (BK), and mass windows (MW) (in units of %). Ellipses mean that the results are 0.

$\sqrt{s}$ (GeV)	Lum	Tracking	Photon	BR	MW	KMFIT	ISR	BK	Total
4.288	1.0	4.0	2.0	1.2	3.6	3.3	3.6	19.5	21.0
4.312	1.0	4.0	2.0	1.2	3.6	3.1	9.7	30.6	32.8
4.337	1.0	4.0	2.0	1.2	3.6	3.8	15.6	45.0	48.2
4.377	1.0	4.0	2.0	1.2	3.6	3.3	18.3	10.7	22.3
4.396	1.0	4.0	2.0	1.2	3.6	3.3	16.9	⋯	18.2
4.436	1.0	4.0	2.0	1.2	3.6	3.2	13.0	10.5	18.0
4.612	1.0	4.0	2.0	1.2	3.6	2.7	5.7	⋯	8.7
4.628	1.0	4.0	2.0	1.2	3.6	3.0	4.2	⋯	7.9
4.641	1.0	4.0	2.0	1.2	3.6	3.0	1.9	20.1	21.3
4.661	1.0	4.0	2.0	1.2	3.6	2.9	7.4	25.9	27.8
4.682	1.0	4.0	2.0	1.2	3.6	2.7	11.6	⋯	13.3
4.699	1.0	4.0	2.0	1.2	3.6	2.7	11.4	40.6	42.7
4.740	1.0	4.0	2.0	1.2	3.6	2.9	8.3	⋯	10.7
4.750	1.0	4.0	2.0	1.2	3.6	2.7	8.4	13.5	17.2
4.781	1.0	4.0	2.0	1.2	3.6	2.5	6.4	⋯	9.1
4.843	1.0	4.0	2.0	1.2	3.6	2.9	3.7	44.4	45.1
4.918	1.0	4.0	2.0	1.2	3.6	2.7	4.5	⋯	8.0
4.951	1.0	4.0	2.0	1.2	3.6	3.0	3.3	⋯	7.4

TABLE X. The systematic uncertainties of $e^+e^- \to \eta\tilde{X}(3872)$ cross section measurement for luminosity, tracking efficiency, photon reconstruction efficiency, branching fraction, η and J/ψ mass windows, kinematic fit, ISR correction factor, background expectation, and sideband regions for settings I and II (in units of %). The total systematic uncertainty is the sum of the individual uncertainties in quadrature. Ellipses mean that the results are 0.

	$\sqrt{s}$ (GeV)	Lum	Tracking	Photon	BR	MW	KMFIT	ISR	BK	Sidebands	Total
Setting I	4.612	1.0	4.0	2.0	0.8	2.8	1.4	3.1	16.9	0.1	18.1
	4.628	1.0	4.0	2.0	0.8	2.8	1.6	1.7	13.8	0.1	15.0
	4.641	1.0	4.0	2.0	0.8	2.8	1.9	1.2	3.2	0.1	6.7
	4.661	1.0	4.0	2.0	0.8	2.8	1.9	7.8	0.7	0.1	9.7
	4.682	1.0	4.0	2.0	0.8	2.8	1.9	11.8	6.0	0.1	14.4
	4.699	1.0	4.0	2.0	0.8	2.8	1.5	9.9	⋯	0.1	11.4
	4.740	1.0	4.0	2.0	0.8	2.8	1.7	7.7	⋯	0.1	9.6
	4.750	1.0	4.0	2.0	0.8	2.8	1.6	8.4	3.7	0.1	10.8
	4.781	1.0	4.0	2.0	0.8	2.8	1.9	6.4	⋯	0.1	8.6
	4.843	1.0	4.0	2.0	0.8	2.8	1.4	4.8	⋯	0.1	7.4
	4.918	1.0	4.0	2.0	0.8	2.8	1.5	3.4	⋯	0.1	6.6
	4.951	1.0	4.0	2.0	0.8	2.8	1.7	5.6	⋯	0.1	8.0
	$\sqrt{s}$ (GeV)	Lum	Tracking	Photon	BR	MW	KMFIT	ISR	BK	Sidebands	Total
Setting II	4.612	1.0	4.0	2.0	0.8	2.8	1.8	3.3	⋯	1.3	6.7
	4.628	1.0	4.0	2.0	0.8	2.8	1.8	1.6	⋯	1.3	6.1
	4.641	1.0	4.0	2.0	0.8	2.8	2.3	0.2	⋯	1.3	6.1
	4.661	1.0	4.0	2.0	0.8	2.8	2.3	6.4	⋯	1.3	8.8
	4.682	1.0	4.0	2.0	0.8	2.8	2.2	10.3	⋯	1.3	12.0
	4.699	1.0	4.0	2.0	0.8	2.8	2.2	9.8	⋯	1.3	11.5
	4.740	1.0	4.0	2.0	0.8	2.8	2.2	7.3	⋯	1.3	9.5
	4.750	1.0	4.0	2.0	0.8	2.8	2.0	6.4	⋯	1.3	8.8
	4.781	1.0	4.0	2.0	0.8	2.8	2.1	6.3	⋯	1.3	8.7
	4.843	1.0	4.0	2.0	0.8	2.8	2.1	4.3	⋯	1.3	7.4
	4.918	1.0	4.0	2.0	0.8	2.8	2.1	3.3	⋯	1.3	6.8
	4.951	1.0	4.0	2.0	0.8	2.8	2.2	4.8	⋯	1.3	7.7

parameters of charged tracks according to the method described in Ref. [62]. The MC sample with the track helix parameter correction is considered as the nominal one. The difference between detection efficiencies obtained from MC samples with and without the correction is taken as the uncertainty. They range from 1.4% to 3.8%.

(vii) Background estimation. The dominant uncertainty for the number of $e^+e^- \to \gamma\gamma\psi(2S)$ background events is statistical only, and it is measured using Eq. (2). For the other background sources, the numbers of events are estimated using Eq. (3). The cross sections mean values for the background are increased by their corresponding uncertainties, resulting in a change of the signal yields. The difference of the signal cross sections due to this change is taken as the uncertainty of the background estimation. The uncertainties range from 0.0% to 45.0% for the $e^+e^- \to \eta\psi(2S)$ and from 0.0% to 16.9% for the $e^+e^- \to \eta\tilde{X}(3872)$ cross section measurements. For some cases, the change does not affect the number of signal events, thus their uncertainty due to background estimation shows zero in Tables VIII and IX.

(viii) Mass window. The systematic uncertainties on J/ψ, η, and $\psi(2S)$ mass windows are 0.9%, 2.6%, and 2.3%, respectively, from Ref. [24]. The total systematic uncertainty on mass windows for the $e^+e^- \to \eta\psi(2S)$ process is 3.6% by adding the three numbers in quadrature, while for the $e^+e^- \to \eta\tilde{X}(3872)$ process is 2.8% summing up quadratically the uncertainties of the J/ψ and η mass windows.

(ix) Sideband region. The systematic uncertainty due to the sideband region for the $e^+e^- \to \eta\tilde{X}(3872)$ cross section measurement is estimated by moving the region of $\pm 0.5\sigma$ of the $\tilde{X}(3872)$ mass. The difference of cross sections is taken as the systematic uncertainty on sideband region.

VI. SUMMARY

In summary, using the new BESIII data samples collected at c.m. energies from 4.288 to 4.951 GeV with an integrated luminosity of about 8.9 fb^{-1}, the process

$e^+e^- \to \eta\psi(2S)$ with $\psi(2S) \to \pi^+\pi^- J/\psi$ has been studied. Due to the limited statistics, upper limits on the cross sections are provided at 90% CL. Combining the current measurement and the previous result from Ref. [24], the total number of observed events at the 32 energy points is 79, and the total number of expected background events is 27 ± 3, corresponding to a P-value of 8.2×10^{-14} for the background-only hypothesis and a statistical significance of 7σ for $e^+e^- \to \eta\psi(2S)$ based on 14.2 fb^{-1} of BESIII data.

In addition, we have searched for signals of the $\tilde{X}(3872)$ with charge conjugate parity $C = -1$ and a mass of 3860.0 ± 10.4 MeV/c^2, as reported by the COMPASS experiment [25] in the $\pi^+\pi^- J/\psi$ invariant mass distribution. We do not find any evident signal for the $\tilde{X}(3872)$, and we set upper limits on the cross sections of $e^+e^- \to \eta\tilde{X}(3872)[\tilde{X}(3872) \to \pi^+\pi^- J/\psi]$ at 90% CL assuming two different width hypotheses, which are consistent with each other.

ACKNOWLEDGMENTS

The BESIII Collaboration thanks the staff of BEPCII and the IHEP computing center for their strong support. This work is supported in part by National Key R&D Program of China under Contracts No. 2020YFA0406300, No. 2020YFA0406400, No. 2023YFA1606000; National Natural Science Foundation of China (NSFC) under Contracts No. 11635010, No. 11735014, No. 11835012, No. 11935015, No. 11935016, No. 11935018, No. 11961141012, No. 12025502, No. 12035009, No. 12035013, No. 12061131003, No. 12192260, No. 12192261, No. 12192262, No. 12192263, No. 12192264, No. 12192265, No. 12221005, No. 12225509, No. 12235017; the Chinese Academy of Sciences (CAS) Large-Scale Scientific Facility Program; the CAS Center for Excellence in Particle Physics (CCEPP); Joint Large-Scale Scientific Facility Funds of the NSFC and CAS under Contract No. U1832207; CAS Key Research Program of Frontier Sciences under Contracts No. QYZDJ-SSW-SLH003, No. QYZDJ-SSW-SLH040; 100 Talents Program of CAS; The Institute of Nuclear and Particle Physics (INPAC) and Shanghai Key Laboratory for Particle Physics and Cosmology; European Union's Horizon 2020 research and innovation program under Marie Sklodowska-Curie Grant Agreement No. 894790; German Research Foundation DFG under Contracts No. 455635585, Collaborative Research Center CRC 1044, No. FOR5327, No. GRK 2149; Istituto Nazionale di Fisica Nucleare, Italy; Ministry of Development of Turkey under Contract No. DPT2006K-120470; National Research Foundation of Korea under Contract No. NRF-2022R1A2C1092335; National Science and Technology fund of Mongolia; National Science Research and Innovation Fund (NSRF) via the Program Management Unit for Human Resources and Institutional Development, Research and Innovation of Thailand under Contract No. B16F640076; Polish National Science Centre under Contract No. 2019/35/O/ST2/02907; the Swedish Research Council; U.S. Department of Energy under Contract No. DE-FG02-05ER41374.

[1] S. K. Choi *et al.* (Belle Collaboration), Observation of a narrow charmoniumlike state in exclusive $B^\pm \to K^\pm\pi^+\pi^- J/\psi$ decays, Phys. Rev. Lett. **91**, 262001 (2003).
[2] N. Brambilla, S. Eidelman, C. Hanhart, A. Nefediev, C. P. Shen, C. E. Thomas, A. Vairo, and C. Z. Yuan, The XYZ states: Experimental and theoretical status and perspectives, Phys. Rep. **873**, 1 (2020).
[3] M. Ablikim *et al.* (BESIII Collaboration), Observation of a near-threshold structure in the K^+ recoil-mass spectra in $e^+e^- \to K^+(D_s^- D^{*0} + D_s^{*-} D^0)$, Phys. Rev. Lett. **126**, 102001 (2021).
[4] T. Barnes, S. Godfrey, and E. S. Swanson, Higher charmonia, Phys. Rev. D **72**, 054026 (2005).
[5] H. X. Chen, W. Chen, X. Liu, and S. L. Zhu, The hidden-charm pentaquark and tetraquark states, Phys. Rep. **639**, 1 (2016).
[6] A. Esposito, A. Pilloni, and A. D. Polosa, Multiquark resonances, Phys. Rep. **668**, 1 (2017).
[7] R. F. Lebed, R. E. Mitchell, and E. S. Swanson, Heavy-quark QCD exotica, Prog. Part. Nucl. Phys. **93**, 143 (2017).
[8] A. Ali, J. S. Lange, and S. Stone, Exotics: Heavy pentaquarks and tetraquarks, Prog. Part. Nucl. Phys. **97**, 123 (2017).
[9] S. L. Olsen, T. Skwarnicki, and D. Zieminska, Nonstandard heavy mesons and baryons: Experimental evidence, Rev. Mod. Phys. **90**, 015003 (2018).
[10] F. K. Guo, C. Hanhart, U. G. Meißner, Q. Wang, Q. Zhao, and B. S. Zou, Hadronic molecules, Rev. Mod. Phys. **90**, 015004 (2018).
[11] B. Aubert *et al.* (*BABAR* Collaboration), Observation of a broad structure in the $\pi^+\pi^- J/\psi$ mass spectrum around 4.26 GeV/c^2, Phys. Rev. Lett. **95**, 142001 (2005).
[12] Q. He *et al.* (CLEO Collaboration), Confirmation of the $Y(4260)$ resonance production in initial state radiation, Phys. Rev. D **74**, 091104(R) (2006).
[13] C. Z. Yuan *et al.* (Belle Collaboration), Measurement of the $e^+e^- \to \pi^+\pi^- J/\psi$ cross section via initial-state radiation at Belle, Phys. Rev. Lett. **99**, 182004 (2007).
[14] J. P. Lees *et al.* (*BABAR* Collaboration), Study of the reaction $e^+e^- \to J/\psi\pi^+\pi^-$ via initial-state radiation at *BABAR*, Phys. Rev. D **86**, 051102(R) (2012).

[15] Z. Q. Liu *et al.* (Belle Collaboration), Study of $e^+e^- \to \pi^+\pi^- J/\psi$ and observation of a charged charmoniumlike state at Belle, Phys. Rev. Lett. **110**, 252002 (2013).

[16] B. Aubert *et al.* (*BABAR* Collaboration), Evidence of a broad structure at an invariant mass of 4.32 GeV/c^2 in the reaction $e^+e^- \to \pi^+\pi^-\psi(2S)$ measured at *BABAR*, Phys. Rev. Lett. **98**, 212001 (2007).

[17] X. L. Wang *et al.* (Belle Collaboration), Observation of two resonant structures in $e^+e^- \to \pi^+\pi^-\psi(2S)$ via initial-state radiation at Belle, Phys. Rev. Lett. **99**, 142002 (2007).

[18] J. P. Lees *et al.* (*BABAR* Collaboration), Study of the reaction $e^+e^- \to \psi(2S)\pi^+\pi^-$ via initial-state radiation at *BABAR*, Phys. Rev. D **89**, 111103(R) (2014).

[19] M. Ablikim *et al.* (BESIII Collaboration), Evidence of a resonant structure in the $e^+e^- \to \pi^+ D^0 D^{*-}$ cross section between 4.05 and 4.60 GeV, Phys. Rev. Lett. **122**, 102002 (2019).

[20] M. Ablikim *et al.* (BESIII Collaboration), Measurement of $e^+e^- \to \pi^+\pi^- D^+ D^-$ cross sections at center-of-mass energies from 4.190 to 4.946 GeV, Phys. Rev. D **106**, 052012 (2022).

[21] S. Jia *et al.* (Belle Collaboration), Evidence for a vector charmoniumlike state in $e^+e^- \to D_s^+ D_{s2}^*(2573)^- + \text{c.c.}$, Phys. Rev. D **101**, 091101(R) (2020).

[22] M. Ablikim *et al.* (BESIII Collaboration), Observation of three charmoniumlike states with $J^{PC} = 1^{--}$ in $e^+e^- \to D^{*0}D^{*-}\pi^+$, Phys. Rev. Lett. **130**, 121901 (2023).

[23] M. Ablikim *et al.* (BESIII Collaboration), Observation of the $Y(4230)$ and a new structure in $e^+e^- \to K^+K^- J/\psi$, Chin. Phys. C **46**, 111002 (2022).

[24] M. Ablikim *et al.* (BESIII Collaboration), Observation of $e^+e^- \to \eta\psi(2S)$ at center-of-mass energies from 4.236 to 4.600 GeV, J. High Energy Phys. 10 (2021) 177.

[25] M. Aghasyan *et al.* (COMPASS Collaboration), Search for muoproduction of $X(3872)$ at COMPASS and indication of a new state $\tilde{X}(3872)$, Phys. Lett. B **783**, 334 (2018).

[26] M. Ablikim *et al.* (BESIII Collaboration), Design and construction of the BESIII detector, Nucl. Instrum. Methods Phys. Res., Sect. A **614**, 345 (2010).

[27] M. Ablikim *et al.* (BESIII Collaboration), Measurements of the center-of-mass energies at BESIII via the di-muon process, Chin. Phys. C **40**, 063001 (2016).

[28] M. Ablikim *et al.* (BESIII Collaboration), Precision measurement of the integrated luminosity of the data taken by BESIII at center-of-mass energies between 3.810 GeV and 4.600 GeV, Chin. Phys. C **39**, 093001 (2015).

[29] M. Ablikim *et al.* (BESIII Collaboration), Luminosity measurements for the R scan experiment at BESIII, Chin. Phys. C **41**, 063001 (2017).

[30] C. H. Yu *et al.*, BEPCII performance and beam dynamics studies on luminosity, in *Proceedings of IPAC2016, Busan, Korea* (2016), http://accelconf.web.cern.ch/ipac2016/doi/JACoW-IPAC2016-TUYA01.html.

[31] M. Ablikim *et al.* (BESIII Collaboration), White paper on the future physics programme of BESIII, Chin. Phys. C **44**, 040001 (2020).

[32] J. Lu, Y. Xiao, and X. Ji, Online monitoring of the center-of-mass energy from real data at BESIII, Radiat. Detect. Technol. Methods **4**, 337 (2020).

[33] J. W. Zhang, L. H. Wu, S. S. Sun *et al.*, Suppression of top-up injection backgrounds with offline event filter in the BESIII experiment, Radiat. Detect. Technol. Methods **6**, 289 (2022).

[34] X. Li *et al.*, Study of MRPC technology for BESIII endcap-TOF upgrade, Radiat. Detect. Technol. Methods **1**, 13 (2017).

[35] Y. X. Guo *et al.*, The study of time calibration for upgraded end cap TOF of BESIII, Radiat. Detect. Technol. Methods **1**, 15 (2017).

[36] P. Cao *et al.*, Design and construction of the new BESIII endcap time-of-flight system with MRPC technology, Nucl. Instrum. Methods Phys. Res., Sect. A **953**, 163053 (2020).

[37] S. Agostinelli *et al.* (GEANT4 Collaboration), Geant4—A simulation toolkit, Nucl. Instrum. Methods Phys. Res., Sect. A **506**, 250 (2003).

[38] S. Jadach, B. F. L. Ward, and Z. Was, The precision Monte Carlo event generator KK for two-fermion final states in e^+e^- collisions, Comput. Phys. Commun. **130**, 260 (2000).

[39] S. Jadach, B. F. L. Ward, and Z. Was, Coherent exclusive exponentiation for precision Monte Carlo calculations, Phys. Rev. D **63**, 113009 (2001).

[40] D. J. Lange, The EvtGen particle decay simulation package, Nucl. Instrum. Methods Phys. Res., Sect. A **462**, 152 (2001).

[41] R. G. Ping, Event generators at BESIII, Chin. Phys. C **32**, 599 (2008).

[42] R. Workman *et al.* (Particle Data Group), The review of particle physics, Prog. Theor. Exp. Phys. **2022**, 083C01 (2022).

[43] J. C. Chen, G. S. Huang, X. R. Qi, D. H. Zhang, and Y. S. Zhu, Event generator for J/ψ and $\psi(2S)$ decay, Phys. Rev. D **62**, 034003 (2000).

[44] R. L. Yang, R. G. Ping, and H. Chen, Tuning and validation of the Lundcharm model with J/ψ decays, Chin. Phys. Lett. **31**, 061301 (2014).

[45] E. Richter-Was, QED bremsstrahlung in semileptonic B and leptonic τ decays, Phys. Lett. B **303**, 163 (1993).

[46] S. Actis *et al.* (Working Group on Radiative Corrections and Monte Carlo Generators for Low Energies), Quest for precision in hadronic cross sections at low energy: Monte Carlo tools vs. experimental data, Eur. Phys. J. C **66**, 585 (2010).

[47] M. Ablikim *et al.* (BESIII Collaboration), Cross section measurements of $e^+e^- \to \omega\chi_{c0}$ from $\sqrt{s} = 4.178$ to 4.278 GeV, Phys. Rev. D **99**, 091103(R) (2019).

[48] M. Ablikim *et al.* (BESIII Collaboration), Measurement of $e^+e^- \to \pi^+\pi^-\psi(3686)$ from 4.008 to 4.600 GeV and observation of a charged structure in the $\pi^\pm\psi(3686)$ mass spectrum, Phys. Rev. D **96**, 032004 (2017).

[49] M. Ablikim *et al.* (BESIII Collaboration), Measurement of $e^+e^- \to \pi^0\pi^0\psi(3686)$ at $\sqrt{s}$ from 4.009 to 4.600 GeV and observation of a neutral charmoniumlike structure, Phys. Rev. D **97**, 052001 (2018).

[50] M. Ablikim *et al.* (BESIII Collaboration), Study of $e^+e^- \to \omega\chi_{cJ}$ at center of mass energies from 4.21 to 4.42 GeV, Phys. Rev. Lett. **114**, 092003 (2015).

[51] M. Ablikim *et al.* (BESIII Collaboration), Observation of $e^+e^- \to \omega\chi_{c1,2}$ near $\sqrt{s} = 4.42$ and 4.6 GeV, Phys. Rev. D **93**, 011102(R) (2016).
[52] M. Ablikim *et al.* (BESIII Collaboration), Observation of structures in the processes $e^+e^- \to \omega\chi_{c1}$ and $\omega\chi_{c2}$, Phys. Rev. Lett. **132**, 161901 (2024).
[53] M. Ablikim *et al.* (BESIII Collaboration), Study of $e^+e^- \to \gamma\omega J/\psi$ and observation of $X(3872) \to \omega J/\psi$, Phys. Rev. Lett. **122**, 232002 (2019).
[54] M. Ablikim *et al.* (BESIII Collaboration), Observation of $e^+e^- \to \phi\chi_{c1}$ and $\phi\chi_{c2}$ at $\sqrt{s} = 4.600$ GeV, Phys. Rev. D **97**, 032008 (2018).
[55] M. Ablikim *et al.* (BESIII Collaboration), Study of $e^+e^- \to \gamma\phi J/\psi$ from $\sqrt{s} = 4.600$ to 4.951 GeV, J. High Energy Phys. 01 (2023) 132.
[56] E. A. Kuraev and V. S. Fadin, On radiative corrections to cross section of e e one-photon annihilation at large energy, Yad. Fiz. **41**, 733 (1985), https://www.osti.gov/etdeweb/biblio/6173920 [Sov. J. Nucl. Phys. **41**, 466 (1985)].
[57] G. J. Feldman and R. D. Cousins. Unified approach to the classical statistical analysis of small signals, Phys. Rev. D **57**, 3873 (1998).
[58] J. Conrad, A program for confidence interval calculations for a Poisson process with background including systematic uncertainties: POLE 1.0, Comput. Phys. Commun. **2**, 158 (2004).
[59] M. Ablikim *et al.* (BESIII Collaboration), Observation of resonance structures in $e^+e^- \to \pi^+\pi^-\psi_2(3823)$ and mass measurement of $\psi_2(3823)$, Phys. Rev. Lett. **129**, 102003 (2022).
[60] M. Ablikim *et al.* (BESIII Collaboration), Observation of $e^+e^- \to \eta' J/\psi$ at center-of-mass energies between 4.189 and 4.600 GeV, Phys. Rev. D **94**, 032009 (2016).
[61] M. Ablikim *et al.* (BESIII Collaboration), Branching fraction measurements of χ_{c0} and χ_{c2} to $\pi^0\pi^0$ and $\eta\eta$, Phys. Rev. D **81**, 052005 (2010).
[62] M. Ablikim *et al.* (BESIII Collaboration), Search for hadronic transition $\chi_{cJ} \to \eta_c\pi^+\pi^-$ and observation of $\chi_{cJ} \to K\bar{K}\pi\pi\pi$, Phys. Rev. D **87**, 012002 (2013).

M. Ablikim,[1] M. N. Achasov,[4,c] P. Adlarson,[75] O. Afedulidis,[3] X. C. Ai,[80] R. Aliberti,[35] A. Amoroso,[74a,74c] Q. An,[71,58,a] Y. Bai,[57] O. Bakina,[36] I. Balossino,[29a] Y. Ban,[46,h] H.-R. Bao,[63] V. Batozskaya,[1,44] K. Begzsuren,[32] N. Berger,[35] M. Berlowski,[44] M. Bertani,[28a] D. Bettoni,[29a] F. Bianchi,[74a,74c] E. Bianco,[74a,74c] A. Bortone,[74a,74c] I. Boyko,[36] R. A. Briere,[5] A. Brueggemann,[68] H. Cai,[76] X. Cai,[1,58] A. Calcaterra,[28a] G. F. Cao,[1,63] N. Cao,[1,63] S. A. Cetin,[62a] J. F. Chang,[1,58] G. R. Che,[43] G. Chelkov,[36,b] C. Chen,[43] C. H. Chen,[9] Chao Chen,[55] G. Chen,[1] H. S. Chen,[1,63] H. Y. Chen,[20] M. L. Chen,[1,58,63] S. J. Chen,[42] S. L. Chen,[45] S. M. Chen,[61] T. Chen,[1,63] X. R. Chen,[31,63] X. T. Chen,[1,63] Y. B. Chen,[1,58] Y. Q. Chen,[34] Z. J. Chen,[25,i] Z. Y. Chen,[1,63] S. K. Choi,[10] G. Cibinetto,[29a] F. Cossio,[74c] J. J. Cui,[50] H. L. Dai,[1,58] J. P. Dai,[78] A. Dbeyssi,[18] R. E. de Boer,[3] D. Dedovich,[36] C. Q. Deng,[72] Z. Y. Deng,[1] A. Denig,[35] I. Denysenko,[36] M. Destefanis,[74a,74c] F. De Mori,[74a,74c] B. Ding,[66,1] X. X. Ding,[46,h] Y. Ding,[40] Y. Ding,[34] J. Dong,[1,58] L. Y. Dong,[1,63] M. Y. Dong,[1,58,63] X. Dong,[76] M. C. Du,[1] S. X. Du,[80] Y. Y. Duan,[55] Z. H. Duan,[42] P. Egorov,[36,b] Y. H. Fan,[45] J. Fang,[59] J. Fang,[1,58] S. S. Fang,[1,63] W. X. Fang,[1] Y. Fang,[1] Y. Q. Fang,[1,58] R. Farinelli,[29a] L. Fava,[74b,74c] F. Feldbauer,[3] G. Felici,[28a] C. Q. Feng,[71,58] J. H. Feng,[59] Y. T. Feng,[71,58] M. Fritsch,[3] C. D. Fu,[1] J. L. Fu,[63] Y. W. Fu,[1,63] H. Gao,[63] X. B. Gao,[41] Y. N. Gao,[46,h] Yang Gao,[71,58] S. Garbolino,[74c] I. Garzia,[29a,29b] L. Ge,[80] P. T. Ge,[76] Z. W. Ge,[42] C. Geng,[59] E. M. Gersabeck,[67] A. Gilman,[69] K. Goetzen,[13] L. Gong,[40] W. X. Gong,[1,58] W. Gradl,[35] S. Gramigna,[29a,29b] M. Greco,[74a,74c] M. H. Gu,[1,58] Y. T. Gu,[15] C. Y. Guan,[1,63] A. Q. Guo,[31,63] L. B. Guo,[41] M. J. Guo,[50] R. P. Guo,[49] Y. P. Guo,[12,g] A. Guskov,[36,b] J. Gutierrez,[27] K. L. Han,[63] T. T. Han,[1] F. Hanisch,[3] X. Q. Hao,[19] F. A. Harris,[65] K. K. He,[55] K. L. He,[1,63] F. H. Heinsius,[3] C. H. Heinz,[35] Y. K. Heng,[1,58,63] C. Herold,[60] T. Holtmann,[3] P. C. Hong,[34] G. Y. Hou,[1,63] X. T. Hou,[1,63] Y. R. Hou,[63] Z. L. Hou,[1] B. Y. Hu,[59] H. M. Hu,[1,63] J. F. Hu,[56,j] S. L. Hu,[12,g] T. Hu,[1,58,63] Y. Hu,[1] G. S. Huang,[71,58] K. X. Huang,[59] L. Q. Huang,[31,63] X. T. Huang,[50] Y. P. Huang,[1] Y. S. Huang,[59] T. Hussain,[73] F. Hölzken,[3] N. Hüsken,[35] N. in der Wiesche,[68] J. Jackson,[27] S. Janchiv,[32] J. H. Jeong,[10] Q. Ji,[1] Q. P. Ji,[19] W. Ji,[1,63] X. B. Ji,[1,63] X. L. Ji,[1,58] Y. Y. Ji,[50] X. Q. Jia,[50] Z. K. Jia,[71,58] D. Jiang,[1,63] H. B. Jiang,[76] P. C. Jiang,[46,h] S. S. Jiang,[39] T. J. Jiang,[16] X. S. Jiang,[1,58,63] Y. Jiang,[63] J. B. Jiao,[50] J. K. Jiao,[34] Z. Jiao,[23] S. Jin,[42] Y. Jin,[66] M. Q. Jing,[1,63] X. M. Jing,[63] T. Johansson,[75] S. Kabana,[33] N. Kalantar-Nayestanaki,[64] X. L. Kang,[9] X. S. Kang,[40] M. Kavatsyuk,[64] B. C. Ke,[80] V. Khachatryan,[27] A. Khoukaz,[68] R. Kiuchi,[1] O. B. Kolcu,[62a] B. Kopf,[3] M. Kuessner,[3] X. Kui,[1,63] N. Kumar,[26] A. Kupsc,[44,75] W. Kühn,[37] J. J. Lane,[67] P. Larin,[18] L. Lavezzi,[74a,74c] T. T. Lei,[71,58] Z. H. Lei,[71,58] M. Lellmann,[35] T. Lenz,[35] C. Li,[43] C. Li,[47] C. H. Li,[39] Cheng Li,[71,58] D. M. Li,[80] F. Li,[1,58] G. Li,[1] H. B. Li,[1,63] H. J. Li,[19] H. N. Li,[56,j] Hui Li,[43] J. R. Li,[61] J. S. Li,[59] K. Li,[1] L. J. Li,[1,63] L. K. Li,[1] Lei Li,[48] M. H. Li,[43] P. R. Li,[38,k,l] Q. M. Li,[1,63] Q. X. Li,[50] R. Li,[17,31] S. X. Li,[12] T. Li,[50] W. D. Li,[1,63] W. G. Li,[1,a] X. Li,[1,63] X. H. Li,[71,58] X. L. Li,[50] X. Y. Li,[1,63] X. Z. Li,[59] Y. G. Li,[46,h] Z. J. Li,[59] Z. Y. Li,[78] C. Liang,[42] H. Liang,[1,63] H. Liang,[71,58] Y. F. Liang,[54] Y. T. Liang,[31,63] G. R. Liao,[14] L. Z. Liao,[50] Y. P. Liao,[1,63] J. Libby,[26] A. Limphirat,[60] C. C. Lin,[55] D. X. Lin,[31,63] T. Lin,[1] B. J. Liu,[1] B. X. Liu,[76] C. Liu,[34] C. X. Liu,[1] F. Liu,[1] F. H. Liu,[53]

Feng Liu,[6] G. M. Liu,[56,j] H. Liu,[38,k,l] H. B. Liu,[15] H. H. Liu,[1] H. M. Liu,[1,63] Huihui Liu,[21] J. B. Liu,[71,58] J. Y. Liu,[1,63] K. Liu,[38,k,l] K. Y. Liu,[40] Ke Liu,[22] L. Liu,[71,58] L. C. Liu,[43] Lu Liu,[43] M. H. Liu,[12,g] P. L. Liu,[1] Q. Liu,[63] S. B. Liu,[71,58] T. Liu,[12,g] W. K. Liu,[43] W. M. Liu,[71,58] X. Liu,[38,k,l] X. Liu,[39] Y. Liu,[80] Y. Liu,[38,k,l] Y. B. Liu,[43] Z. A. Liu,[1,58,63] Z. D. Liu,[9] Z. Q. Liu,[50] X. C. Lou,[1,58,63] F. X. Lu,[59] H. J. Lu,[23] J. G. Lu,[1,58] X. L. Lu,[1] Y. Lu,[7] Y. P. Lu,[1,58] Z. H. Lu,[1,63] C. L. Luo,[41] J. R. Luo,[59] M. X. Luo,[79] T. Luo,[12,g] X. L. Luo,[1,58] X. R. Lyu,[63] Y. F. Lyu,[43] F. C. Ma,[40] H. Ma,[78] H. L. Ma,[1] J. L. Ma,[1,63] L. L. Ma,[50] M. M. Ma,[1,63] Q. M. Ma,[1] R. Q. Ma,[1,63] T. Ma,[71,58] X. T. Ma,[1,63] X. Y. Ma,[1,58] Y. Ma,[46,h] Y. M. Ma,[31] F. E. Maas,[18] M. Maggiora,[74a,74c] S. Malde,[69] Y. J. Mao,[46,h] Z. P. Mao,[1] S. Marcello,[74a,74c] Z. X. Meng,[66] J. G. Messchendorp,[13,64] G. Mezzadri,[29a] H. Miao,[1,63] T. J. Min,[42] R. E. Mitchell,[27] X. H. Mo,[1,58,63] B. Moses,[27] N. Yu. Muchnoi,[4,c] J. Muskalla,[35] Y. Nefedov,[36] F. Nerling,[18,e] L. S. Nie,[20] I. B. Nikolaev,[4,c] Z. Ning,[1,58] S. Nisar,[11,m] Q. L. Niu,[38,k,l] W. D. Niu,[55] Y. Niu,[50] S. L. Olsen,[63] Q. Ouyang,[1,58,63] S. Pacetti,[28b,28c] X. Pan,[55] Y. Pan,[57] A. Pathak,[34] P. Patteri,[28a] Y. P. Pei,[71,58] M. Pelizaeus,[3] H. P. Peng,[71,58] Y. Y. Peng,[38,k,l] K. Peters,[13,e] J. L. Ping,[41] R. G. Ping,[1,63] S. Plura,[35] V. Prasad,[33] F. Z. Qi,[1] H. Qi,[71,58] H. R. Qi,[61] M. Qi,[42] T. Y. Qi,[12,g] S. Qian,[1,58] W. B. Qian,[63] C. F. Qiao,[63] X. K. Qiao,[80] J. J. Qin,[72] L. Q. Qin,[14] L. Y. Qin,[71,58] X. P. Qin,[12,g] X. S. Qin,[50] Z. H. Qin,[1,58] J. F. Qiu,[1] Z. H. Qu,[72] C. F. Redmer,[35] K. J. Ren,[39] A. Rivetti,[74c] M. Rolo,[74c] G. Rong,[1,63] Ch. Rosner,[18] S. N. Ruan,[43] N. Salone,[44] A. Sarantsev,[36,d] Y. Schelhaas,[35] K. Schoenning,[75] M. Scodeggio,[29a] K. Y. Shan,[12,g] W. Shan,[24] X. Y. Shan,[71,58] Z. J. Shang,[38,k,l] J. F. Shangguan,[16] L. G. Shao,[1,63] M. Shao,[71,58] C. P. Shen,[12,g] H. F. Shen,[1,8] W. H. Shen,[63] X. Y. Shen,[1,63] B. A. Shi,[63] H. Shi,[71,58] H. C. Shi,[71,58] J. L. Shi,[12,g] J. Y. Shi,[1] Q. Q. Shi,[55] S. Y. Shi,[72] X. Shi,[1,58] J. J. Song,[19] T. Z. Song,[59] W. M. Song,[34,1] Y. J. Song,[12,g] Y. X. Song,[46,h,n] S. Sosio,[74a,74c] S. Spataro,[74a,74c] F. Stieler,[35] Y. J. Su,[63] G. B. Sun,[76] G. X. Sun,[1] H. Sun,[63] H. K. Sun,[1] J. F. Sun,[19] K. Sun,[61] L. Sun,[76] S. S. Sun,[1,63] T. Sun,[51,f] W. Y. Sun,[34] Y. Sun,[9] Y. J. Sun,[71,58] Y. Z. Sun,[1] Z. Q. Sun,[1,63] Z. T. Sun,[50] C. J. Tang,[54] G. Y. Tang,[1] J. Tang,[59] M. Tang,[71,58] Y. A. Tang,[76] L. Y. Tao,[72] Q. T. Tao,[25,i] M. Tat,[69] J. X. Teng,[71,58] V. Thoren,[75] W. H. Tian,[59] Y. Tian,[31,63] Z. F. Tian,[76] I. Uman,[62b] Y. Wan,[55] S. J. Wang,[50] B. Wang,[1] B. L. Wang,[63] Bo Wang,[71,58] D. Y. Wang,[46,h] F. Wang,[72] H. J. Wang,[38,k,l] J. J. Wang,[76] J. P. Wang,[50] K. Wang,[1,58] L. L. Wang,[1] M. Wang,[50] N. Y. Wang,[63] S. Wang,[12,g] S. Wang,[38,k,l] T. Wang,[12,g] T. J. Wang,[43] W. Wang,[72] W. Wang,[59] W. P. Wang,[35,71,o] X. Wang,[46,h] X. F. Wang,[38,k,l] X. J. Wang,[39] X. L. Wang,[12,g] X. N. Wang,[1] Y. Wang,[61] Y. D. Wang,[45] Y. F. Wang,[1,58,63] Y. L. Wang,[19] Y. N. Wang,[45] Y. Q. Wang,[1] Yaqian Wang,[17] Yi Wang,[61] Z. Wang,[1,58] Z. L. Wang,[72] Z. Y. Wang,[1,63] Ziyi Wang,[63] D. H. Wei,[14] F. Weidner,[68] S. P. Wen,[1] Y. R. Wen,[39] U. Wiedner,[3] G. Wilkinson,[69] M. Wolke,[75] L. Wollenberg,[3] C. Wu,[39] J. F. Wu,[1,8] L. H. Wu,[1] L. J. Wu,[1,63] X. Wu,[12,g] X. H. Wu,[34] Y. Wu,[71,58] Y. H. Wu,[55] Y. J. Wu,[31] Z. Wu,[1,58] L. Xia,[71,58] X. M. Xian,[39] B. H. Xiang,[1,63] T. Xiang,[46,h] D. Xiao,[38,k,l] G. Y. Xiao,[42] S. Y. Xiao,[1] Y. L. Xiao,[12,g] Z. J. Xiao,[41] C. Xie,[42] X. H. Xie,[46,h] Y. Xie,[50] Y. G. Xie,[1,58] Y. H. Xie,[6] Z. P. Xie,[71,58] T. Y. Xing,[1,63] C. F. Xu,[1,63] C. J. Xu,[59] G. F. Xu,[1] H. Y. Xu,[66,2,p] M. Xu,[71,58] Q. J. Xu,[16] Q. N. Xu,[30] W. Xu,[1] W. L. Xu,[66] X. P. Xu,[55] Y. C. Xu,[77] Z. P. Xu,[42] Z. S. Xu,[63] F. Yan,[12,g] L. Yan,[12,g] W. B. Yan,[71,58] W. C. Yan,[80] X. Q. Yan,[1] H. J. Yang,[51,f] H. L. Yang,[34] H. X. Yang,[1] T. Yang,[1] Y. Yang,[12,g] Y. F. Yang,[43] Y. F. Yang,[1,63] Y. X. Yang,[1,63] Z. W. Yang,[38,k,l] Z. P. Yao,[50] M. Ye,[1,58] M. H. Ye,[8] J. H. Yin,[1] Z. Y. You,[59] B. X. Yu,[1,58,63] C. X. Yu,[43] G. Yu,[1,63] J. S. Yu,[25,i] T. Yu,[72] X. D. Yu,[46,h] Y. C. Yu,[80] C. Z. Yuan,[1,63] J. Yuan,[45] J. Yuan,[34] L. Yuan,[2] S. C. Yuan,[1,63] Y. Yuan,[1,63] Z. Y. Yuan,[59] C. X. Yue,[39] A. A. Zafar,[73] F. R. Zeng,[50] S. H. Zeng,[72] X. Zeng,[12,g] Y. Zeng,[25,i] Y. J. Zeng,[1,63] Y. J. Zeng,[59] X. Y. Zhai,[34] Y. C. Zhai,[50] Y. H. Zhan,[59] A. Q. Zhang,[1,63] B. L. Zhang,[1,63] B. X. Zhang,[1] D. H. Zhang,[43] G. Y. Zhang,[19] H. Zhang,[80] H. Zhang,[71,58] H. C. Zhang,[1,58,63] H. H. Zhang,[59] H. H. Zhang,[34] H. Q. Zhang,[1,58,63] H. R. Zhang,[71,58] H. Y. Zhang,[1,58] J. Zhang,[80] J. Zhang,[59] J. J. Zhang,[52] J. L. Zhang,[20] J. Q. Zhang,[41] J. S. Zhang,[12,g] J. W. Zhang,[1,58,63] J. X. Zhang,[38,k,l] J. Y. Zhang,[1] J. Z. Zhang,[1,63] Jianyu Zhang,[63] L. M. Zhang,[61] Lei Zhang,[42] P. Zhang,[1,63] Q. Y. Zhang,[34] R. Y. Zhang,[38,k,l] S. H. Zhang,[1,63] Shulei Zhang,[25,i] X. D. Zhang,[45] X. M. Zhang,[1] X. Y. Zhang,[50] Y. Zhang,[72] Y. Zhang,[1] Y. T. Zhang,[80] Y. H. Zhang,[1,58] Y. M. Zhang,[39] Yan Zhang,[71,58] Z. D. Zhang,[1] Z. H. Zhang,[1] Z. L. Zhang,[34] Z. Y. Zhang,[43] Z. Y. Zhang,[76] Z. Z. Zhang,[45] G. Zhao,[1] J. Y. Zhao,[1,63] J. Z. Zhao,[1,58] L. Zhao,[1] Lei Zhao,[71,58] M. G. Zhao,[43] N. Zhao,[78] R. P. Zhao,[63] S. J. Zhao,[80] Y. B. Zhao,[1,58] Y. X. Zhao,[31,63] Z. G. Zhao,[71,58] A. Zhemchugov,[36,b] B. Zheng,[72] B. M. Zheng,[34] J. P. Zheng,[1,58] W. J. Zheng,[1,63] Y. H. Zheng,[63] B. Zhong,[41] X. Zhong,[59] H. Zhou,[50] J. Y. Zhou,[34] L. P. Zhou,[1,63] S. Zhou,[6] X. Zhou,[76] X. K. Zhou,[6] X. R. Zhou,[71,58] X. Y. Zhou,[39] Y. Z. Zhou,[12,g] J. Zhu,[43] K. Zhu,[1] K. J. Zhu,[1,58,63] K. S. Zhu,[12,g] L. Zhu,[34] L. X. Zhu,[63] S. H. Zhu,[70] S. Q. Zhu,[42] T. J. Zhu,[12,g] W. D. Zhu,[41] Y. C. Zhu,[71,58] Z. A. Zhu,[1,63] J. H. Zou,[1] and J. Zu[71,58]

(BESIII Collaboration)

[1]*Institute of High Energy Physics, Beijing 100049, People's Republic of China*
[2]*Beihang University, Beijing 100191, People's Republic of China*
[3]*Bochum Ruhr-University, D-44780 Bochum, Germany*
[4]*Budker Institute of Nuclear Physics SB RAS (BINP), Novosibirsk 630090, Russia*
[5]*Carnegie Mellon University, Pittsburgh, Pennsylvania 15213, USA*
[6]*Central China Normal University, Wuhan 430079, People's Republic of China*
[7]*Central South University, Changsha 410083, People's Republic of China*
[8]*China Center of Advanced Science and Technology, Beijing 100190, People's Republic of China*
[9]*China University of Geosciences, Wuhan 430074, People's Republic of China*
[10]*Chung-Ang University, Seoul 06974, Republic of Korea*
[11]*COMSATS University Islamabad, Lahore Campus,*
Defence Road, Off Raiwind Road, 54000 Lahore, Pakistan
[12]*Fudan University, Shanghai 200433, People's Republic of China*
[13]*GSI Helmholtzcentre for Heavy Ion Research GmbH, D-64291 Darmstadt, Germany*
[14]*Guangxi Normal University, Guilin 541004, People's Republic of China*
[15]*Guangxi University, Nanning 530004, People's Republic of China*
[16]*Hangzhou Normal University, Hangzhou 310036, People's Republic of China*
[17]*Hebei University, Baoding 071002, People's Republic of China*
[18]*Helmholtz Institute Mainz, Staudinger Weg 18, D-55099 Mainz, Germany*
[19]*Henan Normal University, Xinxiang 453007, People's Republic of China*
[20]*Henan University, Kaifeng 475004, People's Republic of China*
[21]*Henan University of Science and Technology, Luoyang 471003, People's Republic of China*
[22]*Henan University of Technology, Zhengzhou 450001, People's Republic of China*
[23]*Huangshan College, Huangshan 245000, People's Republic of China*
[24]*Hunan Normal University, Changsha 410081, People's Republic of China*
[25]*Hunan University, Changsha 410082, People's Republic of China*
[26]*Indian Institute of Technology Madras, Chennai 600036, India*
[27]*Indiana University, Bloomington, Indiana 47405, USA*
[28a]*INFN Laboratori Nazionali di Frascati, I-00044, Frascati, Italy*
[28b]*INFN Sezione di Perugia, I-06100, Perugia, Italy*
[28c]*University of Perugia, I-06100, Perugia, Italy*
[29a]*INFN Sezione di Ferrara, I-44122, Ferrara, Italy*
[29b]*University of Ferrara, I-44122, Ferrara, Italy*
[30]*Inner Mongolia University, Hohhot 010021, People's Republic of China*
[31]*Institute of Modern Physics, Lanzhou 730000, People's Republic of China*
[32]*Institute of Physics and Technology, Peace Avenue 54B, Ulaanbaatar 13330, Mongolia*
[33]*Instituto de Alta Investigación, Universidad de Tarapacá, Casilla 7D, Arica 1000000, Chile*
[34]*Jilin University, Changchun 130012, People's Republic of China*
[35]*Johannes Gutenberg University of Mainz, Johann-Joachim-Becher-Weg 45, D-55099 Mainz, Germany*
[36]*Joint Institute for Nuclear Research, 141980 Dubna, Moscow region, Russia*
[37]*Justus-Liebig-Universitaet Giessen, II. Physikalisches Institut,*
Heinrich-Buff-Ring 16, D-35392 Giessen, Germany
[38]*Lanzhou University, Lanzhou 730000, People's Republic of China*
[39]*Liaoning Normal University, Dalian 116029, People's Republic of China*
[40]*Liaoning University, Shenyang 110036, People's Republic of China*
[41]*Nanjing Normal University, Nanjing 210023, People's Republic of China*
[42]*Nanjing University, Nanjing 210093, People's Republic of China*
[43]*Nankai University, Tianjin 300071, People's Republic of China*
[44]*National Centre for Nuclear Research, Warsaw 02-093, Poland*
[45]*North China Electric Power University, Beijing 102206, People's Republic of China*
[46]*Peking University, Beijing 100871, People's Republic of China*
[47]*Qufu Normal University, Qufu 273165, People's Republic of China*
[48]*Renmin University of China, Beijing 100872, People's Republic of China*
[49]*Shandong Normal University, Jinan 250014, People's Republic of China*
[50]*Shandong University, Jinan 250100, People's Republic of China*
[51]*Shanghai Jiao Tong University, Shanghai 200240, People's Republic of China*
[52]*Shanxi Normal University, Linfen 041004, People's Republic of China*
[53]*Shanxi University, Taiyuan 030006, People's Republic of China*
[54]*Sichuan University, Chengdu 610064, People's Republic of China*

[55]*Soochow University, Suzhou 215006, People's Republic of China*
[56]*South China Normal University, Guangzhou 510006, People's Republic of China*
[57]*Southeast University, Nanjing 211100, People's Republic of China*
[58]*State Key Laboratory of Particle Detection and Electronics, Beijing 100049, Hefei 230026, People's Republic of China*
[59]*Sun Yat-Sen University, Guangzhou 510275, People's Republic of China*
[60]*Suranaree University of Technology, University Avenue 111, Nakhon Ratchasima 30000, Thailand*
[61]*Tsinghua University, Beijing 100084, People's Republic of China*
[62a]*Turkish Accelerator Center Particle Factory Group, Istinye University, 34010, Istanbul, Turkey*
[62b]*Near East University, Nicosia, North Cyprus, 99138, Mersin 10, Turkey*
[63]*University of Chinese Academy of Sciences, Beijing 100049, People's Republic of China*
[64]*University of Groningen, NL-9747 AA Groningen, The Netherlands*
[65]*University of Hawaii, Honolulu, Hawaii 96822, USA*
[66]*University of Jinan, Jinan 250022, People's Republic of China*
[67]*University of Manchester, Oxford Road, Manchester, M13 9PL, United Kingdom*
[68]*University of Muenster, Wilhelm-Klemm-Strasse 9, 48149 Muenster, Germany*
[69]*University of Oxford, Keble Road, Oxford OX13RH, United Kingdom*
[70]*University of Science and Technology Liaoning, Anshan 114051, People's Republic of China*
[71]*University of Science and Technology of China, Hefei 230026, People's Republic of China*
[72]*University of South China, Hengyang 421001, People's Republic of China*
[73]*University of the Punjab, Lahore-54590, Pakistan*
[74a]*University of Turin and INFN, I-10125, Turin, Italy*
[74b]*University of Eastern Piedmont, I-15121, Alessandria, Italy*
[74c]*INFN, I-10125, Turin, Italy*
[75]*Uppsala University, Box 516, SE-75120 Uppsala, Sweden*
[76]*Wuhan University, Wuhan 430072, People's Republic of China*
[77]*Yantai University, Yantai 264005, People's Republic of China*
[78]*Yunnan University, Kunming 650500, People's Republic of China*
[79]*Zhejiang University, Hangzhou 310027, People's Republic of China*
[80]*Zhengzhou University, Zhengzhou 450001, People's Republic of China*

[a]Deceased.
[b]Also at the Moscow Institute of Physics and Technology, Moscow 141700, Russia.
[c]Also at the Novosibirsk State University, Novosibirsk 630090, Russia.
[d]Also at the NRC "Kurchatov Institute," PNPI, 188300 Gatchina, Russia.
[e]Also at Goethe University Frankfurt, 60323 Frankfurt am Main, Germany.
[f]Also at Key Laboratory for Particle Physics, Astrophysics and Cosmology, Ministry of Education; Shanghai Key Laboratory for Particle Physics and Cosmology; Institute of Nuclear and Particle Physics, Shanghai 200240, People's Republic of China.
[g]Also at Key Laboratory of Nuclear Physics and Ion-beam Application (MOE) and Institute of Modern Physics, Fudan University, Shanghai 200443, People's Republic of China.
[h]Also at State Key Laboratory of Nuclear Physics and Technology, Peking University, Beijing 100871, People's Republic of China.
[i]Also at School of Physics and Electronics, Hunan University, Changsha 410082, China.
[j]Also at Guangdong Provincial Key Laboratory of Nuclear Science, Institute of Quantum Matter, South China Normal University, Guangzhou 510006, China.
[k]Also at MOE Frontiers Science Center for Rare Isotopes, Lanzhou University, Lanzhou 730000, People's Republic of China.
[l]Also at Lanzhou Center for Theoretical Physics, Lanzhou University, Lanzhou 730000, People's Republic of China.
[m]Also at the Department of Mathematical Sciences, IBA, Karachi 75270, Pakistan.
[n]Also at Ecole Polytechnique Federale de Lausanne (EPFL), CH-1015 Lausanne, Switzerland.
[o]Also at Helmholtz Institute Mainz, Staudinger Weg 18, D-55099 Mainz, Germany.
[p]Also at School of Physics, Beihang University, Beijing 100191, China.